# AN ABSTRACT OF THE THESIS OF

Chianna M. Alexander for the degree of Master of Science in Electrical And Computer Engineering presented on September 16, 2011.

Title: Wind Ramp Prediction.

Abstract approved:

---

Ted K.A. Brekken

The number of wind turbines and wind farms in the Pacific Northwest has increased dramatically in the past six years, which represents a significant amount of electrical generation capacity connected to the public electric grid. However, the variable nature of wind sometimes introduces excessive power, or conversely shortages, in power delivery from the wind farm possibly leading to grid instability in the region. Knowing the short-term wind profile for a wind farm would allow system operators to better schedule generation resources yielding better grid stability.

This thesis presents a method for predicting the power output of a Pacific Northwest Wind Farm by using data collected from wind anemometers located at the wind farm and from off-site meteorological stations. An auto-regressive moving average model (ARMA) with wind velocity inputs from off-site meteorological stations along with current and past wind velocities from the wind farm was used to predict wind velocity changes up to two hours in advance. The predicted wind velocities were then used to compute the future wind farm power output. A fuzzy logic inference system (FLIS)

was used to detect and classify wind power ramps. The FLIS provides outputs indicating the degree of membership of power ramps from 10 to 50% of the nameplate rating of the wind farm. Wind Power Ramp prediction capability will allow system operators better management of the grid and reserve generation resources.

Wind Ramp Prediction

by
Chianna M. Alexander

A THESIS

Submitted to

Oregon State University

in partial fulfillment of
the requirements for the
degree of

Master of Science

Presented September 16, 2011
Commencement June 2012

Master of Science thesis of Chianna M. Alexander presented on September 16, 2011

APPROVED:

Major Professor, representing Electrical and Computer Engineering

Director of the School of Electrical Engineering and Computer Science

Dean of the Graduate School

I understand that my thesis will become part of the permanent collection of Oregon State University libraries. My signature below authorizes release of my thesis to any reader upon request.

Chianna M. Alexander, Author

ACKNOWLEDGEMENTS

I would like thank my advisor, Dr. Ted Brekken, for his patient and thoughtful guidance throughout this research project. I would also like to thank the members of my research group Dr. Yokochi, and Dr. von Jouanne for their valuable input, and to the rest of the members of the team I extend my thanks to Hai-Yue Han, David Naviaux, Alex Bistrika and Eunice Naswalie. To the energy systems graduate students, I would like to thank you for creating an amazing work environment.

# CONTRIBUTION OF AUTHORS

Dr. Ted Brekken provided instruction on how to model the wind speed using autoregressive equations and how to extend the equations to an autoregression moving average model.

TABLE OF CONTENTS

Page

1 Introduction ........ 1

1.1 Research Overview ........ 3

2 Modeling Overview ........ 5

2.1 Persistence Model ........ 5

2.2 Very Short Term Models ........ 5

2.3 Meteorological Stations ........ 7

2.4 Time Series Data Sets ........ 7

2.5 Wind Speed Height Adjustment ........ 8

2.6 Wind Direction ........ 10

3 Wind Speed Prediction ........ 11

3.1 Model Training ........ 12

3.1.1 Coefficient Generation ........ 12

3.1.2 Training Length ........ 12

3.1.3 Filter Order ........ 16

3.2 AR and ARMA Models ........ 16

3.3 Model 0 ........ 19

TABLE OF CONTENTS (continued)

Page


3.3.1 Model 0 Results ........ 20

3.4 Model 1 ........ 23

3.4.1 Model 1 Results ........ 27

3.5 Model 2 ........ 30

3.5.1 Model 2 Results ........ 31

3.6 Model 3 ........ 33

3.6.1 Model 3 Results ........ 37

3.6.2 Model Conclusions ........ 40

4 Wind Speed to Power Conversion ........ 43

4.1 Wind Power Ramp Profiles ........ 44

4.2 Definition: Wind Power Ramp ........ 46

4.3 Power Ramp Rate ........ 48

5 Fuzzy Inference System ........ 49

5.1 Overview ........ 49

5.2 The Power Ramp Detector ........ 50

5.3 Fuzzy Detector Results ........ 52

6 Conclusion ........ 56

TABLE OF CONTENTS (continued)

Page

6.1 Next steps ........................................ 56

BIBLIOGRAPHY ........................................ 58

LIST OF FIGURES

Figure Page

Figure 1.1.1:Wind Power Ramp Prediction Block Diagram ........................................ 3

Figure 1.2: PNWWF and MetStations Location ........................................................... 3

Figure 3.1:Model 0, Train 144 ....................................................................................... 13

Figure 3.2: Model 0, Train 144, Longer Time Interval ................................................ 14

Figure 3.3: Model 0, Train 144 ..................................................................................... 15

Figure 3.4:Model 0 Train 1728 ..................................................................................... 15

Figure 3.5: Model 0 Train 5760 .................................................................................... 15

Figure 3.6: Extreme Wind Ramp Event ....................................................................... 18

Figure 3.7: Medium Wind Ramp Event ....................................................................... 19

Figure 3.8: Model 0, Horizon 6, Medium Ramp Event ............................................... 22

Figure 3.9: Model 0 Horizon 6 Extreme Ramp Event ................................................. 22

Figure 3.10: Model 1, Horizon 6, Medium Ramp Event ............................................. 29

Figure 3.11:Model 1, Horizon 6, Extreme Ramp Event .............................................. 30

Figure 3.12:Model 2, Horizon 6, Medium Ramp Event .............................................. 32

Figure 3.13: Model 2, Horizon 6, Extreme Ramp Event ............................................. 33

Figure 3.14: Model 1 vs. Model 3 ................................................................................. 38

Figure 3.15: Model 3 Medium Ramp Event ................................................................ 39

Figure 3.16: Model 3 Extreme Ramp Event ................................................................ 39

Figure 3.17: Extreme Ramp and Wind Directions ...................................................... 41

LIST OF FIGURES (continued)

Figure Page
Figure 3.18: Model 1 vs. Model 1A Extreme Ramp Event ........................................ 41

Figure 3.19: Model 1 vs. Model 1C Medium Ramp Event......................................... 42

Figure 4.1: Wind Turbine Power Curve........................................................................ 43

Figure 4.2:Power Prediction, Horizon 6 ....................................................................... 45

Figure 4.3: Power Prediction, Horizon 12 .................................................................... 46

Figure 5.1: Fuzzy Inference Architecture ..................................................................... 50

Figure 5.2: Input Membership Functions....................................................................... 51

Figure 5.3: Output Membership Function..................................................................... 51

Figure 5.4: Power Ramp Detection, Horizon 6............................................................. 53

Figure 5.5: Power Ramp Detection, Horizon 12, Extreme Ramp Event ...................... 53

Figure 5.6: Extreme Ramp Recovery Detection, Horizon 6 ......................................... 54

Figure 5.7: Ramp Detection, Horizon 6, Medium Ramp Event .................................. 54

LIST OF TABLES

Table Page

Table 2.1: Distance and Angle to PNWWF .......... 7

Table 2.2: Surface Roughness Values .......... 9

Table 2.3: BPA MetStations Wind Speed Scale Factor .......... 9

Table 2.4: Wind Direction Survey Results .......... 10

Table 3.1: Model 1, 2, 3 Characteristics .......... 16

Table 3.2: MSE Model 0 .......... 21

Table 3.3: MSE Model 1 .......... 28

Table 3.4: Model 2 MSE .......... 32

Table 3.5: Model 3 MSE Model 3 .......... 37

Table 4.1: MAE Power Prediction .......... 45

# 1 Introduction

Wind energy in the Pacific Northwest has grown dramatically in the last six years. In 2005 there was a little more than 250 MW of installed generation capacity in the Bonneville Power Administration (BPA) Balancing Authority Area and in 2011 the installed generation capacity has grown to 3522 MW [1]. Wind energy is providing a significant part of the energy needs for the Pacific Northwest, when there is wind. The electrical grid is a continuous balance between generation and consumption and when large amounts of power from the wind farms are unavailable due to meteorological conditions, the balance must be restored from a spinning reserve source such as hydro or thermal generation. Slow changing --increasing or decreasing-- wind conditions can be compensated for by grid system operators by adjusting the base load power generation. If the wind velocity is fast changing --increasing or decreasing-- and is of sufficient magnitude and duration the resulting change in power could lead to grid instabilities. To ensure grid stability, the balancing authority must hold additional spinning reserves to meet a decreasing generation from wind farm production, or must remove power from base load generation when a wind farm suddenly increases in generation. This is costly because the generation units are running and expending energy but not producing electricity. Also the maintenance interval is shortened adding to the increased cost.

A sudden wind velocity change --increase or decrease-- that has sufficient magnitude and duration is called a wind ramp. The definition of a wind ramp will be discussed in section 4.2.

One solution being investigated by the Wallace Energy Systems and Renewable Facility (WESRF) at Oregon State University is an energy storage system (ESS)[2]. An ESS located on-site at a wind farm will work in conjunction with the wind farm power system to absorb energy during periods that there is either excessive or insufficient energy generated. The goal of the system is to optimize the energy production from the wind farm and minimize stresses placed on the spinning reserve generation sources.

The ESS at WESRF uses a Zinc-Bromide flow cell battery for bulk storage in conjunction with super-capacitors to provide fast response to changing power generation conditions at a wind farm. The batteries, capacitors, and power converters are connected to an in-lab research grid. A control system will manage the charge and discharge of the ESS based upon the state-of-charge (SoC) of the batteries, SoC of the capacitors, demand on the grid, and the projected wind farm output computed from the predicted wind velocity. Predicting the wind velocity, and consequently the wind farm output power provides information to the ESS control system regarding future power output of the wind farm based upon the wind velocity input. Knowing this future power output the control system might issue a command to charge, discharge, or hold the same (no action) to the battery and/or the super-capacitors.

## 1.1 Research Overview

Managing the charge and discharge cycles of an ESS can be more effective if forward-looking knowledge of wind farm production were available. The focus of this research is to provide a method to predict and provide an indication of wind power ramp events. The signal processing flow is shown in Figure 1.1.1.

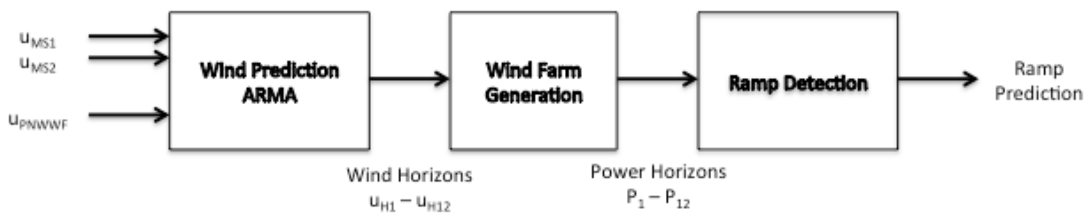


Figure 1.1.1:Wind Power Ramp Prediction Block Diagram

The wind prediction stage is an autoregressive moving average (ARMA) model that uses wind speed data from a Pacific Northwest Wind Farm (PNWWF) along with wind speed data from external Bonneville Power Administration (BPA) meteorological stations (MS1 & MS2).

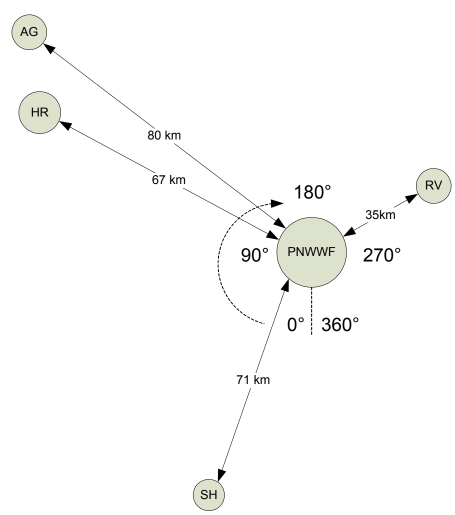


Figure 1.2: PNWWF and MetStations Location

The BPA meteorological stations (MetStations) Figure 1.2 are in close proximity (35-80km) to the wind farm and are sufficiently angularly spaced to account for a large percentage of wind blowing past the MetStation to the wind farm.

Two of the meteorological stations are aligned such that about 50% of the time the wind travels past both stations towards the wind farm. When the directions are concurrent from the meteorological stations the input data from the second MetStation, MS2, is used in the ARMA model.

The wind farm generation stage converts each of the wind speed horizons to total wind farm power output horizons using a turbine power curve modified for aggregated output (discussed later) when given an averaged wind speed input. The power ramp detection is accomplished using a fuzzy inference system that provides an indication of the duration and intensity of a detected power ramp.

# 2 Modeling Overview

Before discussing the ARMA models some background information is presented to give an understanding of previous work. Also discussed are the physical aspects of where the data came from, how the data were modified and the relationship between the different data sets.

## 2.1 Persistence Model

The persistence model (PM) uses the current value as the prediction for all future horizons.

$$y(k+h) = y(k) \quad ; h = 1,2,...n \tag{1}$$

It is a simple model yet performs well is the benchmark for measuring performance.

## 2.2 Very Short Term Models

Due to the dynamic nature of the wind, trying to model this ever-changing fluid is a tremendous challenge in the wind power industry today. Wind velocities are influenced by a variety of physical processes and Numerical Weather Prediction (NWP) is a class of meteorological modeling that utilizes the physical processes in developing a forecast. NWP has been found to be useful for developing forecasts for the short term and longer predictions.

Time frame definitions do not have crisply defined edges in the literature. Short term forecasting is considered to be approximately two to twelve hours, where shorter than two hours is very short term and greater than twelve hours is deemed long term[3][4][5]. Soman et al. has put forth a classification table and definitions in their review of wind speed forecasting [6]. Classification of the time frames is of interest only in identifying the mathematical methods used in making a prediction because most methods are based on time series measurements of wind velocity and direction. For the purposes of this research, the smallest time period is 10 minutes dictated by the sampling rate of the wind anemometers. A two-hour time period for the upper limit of the model fits well with the energy delivery from the batteries in the ESS, and would also allow sufficient time for balancing authority system operators to schedule reserve resources. The 10 minute to 2 hour time period fits within the very short-term definition.

ARMA models are well suited for processing time series data and consequently are a reasonable choice to model wind data. Rajagopalan and Santoso used an ARMA used a single series data set (wind data from a single location) to predict 30 minute to 3 hour horizons and were able to predict a one hour horizon to within 25% error, approximately 45% of the time[7]. Potter and Negnevitsky used an adaptive neuro-fuzzy inference system and demonstrated improved performance over the persistence model for a 2.5-minute horizon[5]. Miranda and Dunn used a Bayesian inference approach to model autoregression for a one-hour forecast and concluded that the performance was marginally better than the persistence model[8]. Torres et al. preprocessed wind data that was sampled at ten-minute intervals and created samples that were hourly averages.  The ARMA model was used on the one-hour data and was able to forecast up to 10 hours in advance and performed better than the persistence model[9]. Other ARMA models that have been used to predict very short term wind velocities are detailed in [10][11][12].

## 2.3 Meteorological Stations

Inputs into the ARMA model, Figure 1.1.1 are time series data from external meteorological stations and the wind farm. The spatial relationship between the weather stations and the wind farm is listed in Table 2.1 and the angle that is listed is based upon BPA's defined direction in the time series for the meteorological data.

Table 2.1: Distance and Angle to PNWWF

| Meteorological Station | Distance (km) | Angle (degrees) |
|---|---|---|
| Augspurger (AG) | 81 | 277 |
| Hood River (HR) | 67 | 274 |
| Shaniko (SH) | 71 | 192 |
| Roosevelt (RV) | 35 | 68 |

## 2.4 Time Series Data Sets

The BPA data were date and time stamped starting from February 1, 2010 at 8:00am UTC. Data were recorded at five-minute intervals and contained wind speed, direction, barometric pressure, relative humidity, and temperature. The PNWWF data contained wind speed and turbine output for each turbine in the wind farm and were recorded at 10-minute intervals. The BPA and PNWWF data contained randomly located corrupt data values. The corrupted data were replaced by a linear value based upon the last known and the next known valid data sample. Once the BPA data were repaired the time series was down-sampled to a ten-minute sampling rate.

The directional data in the BPA time series was processed to develop a digital indicator signal that outputted a one when the wind was traveling in a direction towards the wind farm and a zero otherwise. Table 2.1 gives the actual angle, but the nature of wind is not always consistent; therefore an acceptance angle of ±30° was added to the actual angle when determining the digital indicator. A separate digital indicator was created for each of the meteorological stations in Table 2.1.

## 2.5 Wind Speed Height Adjustment

The wind speed will vary with height and any measured wind speed should be adjusted to account for measurement variations. Wind flowing near the earth will be moving slower than wind at higher elevations. Surface roughness has a significant affect on ground or lower elevation wind speed. Andrews and Jelley [13] gives the relationship of wind velocity as a function of measurement height in (2).

$$u(z) = u_{MS}\left(\frac{z_{HUB}}{z_{MS}}\right)^{\alpha_{MS}} \tag{2}$$

The expression $\left(\frac{z_{HUB}}{z_{MS}}\right)^{\alpha_{MS}}$ from the above equation is a scale factor applied to the wind data before computing wind horizons. The wind shear coefficient $\alpha_{MS}$ is dependent upon the surface roughness and the measured height at the MetStation.

$$\alpha_{MS} = \frac{1}{2}\left(\frac{z_0}{z_{MS}}\right) \tag{3}$$

Where $z_0$ is the surface roughness and $z_{MS}$ is the height of the anemometer above ground level.

Values for surface roughness, $z_0$, vary depending on the surface conditions and Table 2.2 [13] gives ranges of $z_0$ for different terrain.

Table 2.2: Surface Roughness Values

| Terrain | $z_0$ (m) |
|---|---|
| Urban areas | 3 – 0.4 |
| Farmland | 0.3 – 0.002 |
| Open Sea | 0.000 – 0.0001 |

The Hood River MetStation is located in a substation near the city of Hood River with farmland and residential housing nearby so a 0.4 is selected for this location. Augspurger MetStation is located on high mountain ridge, however, there is higher elevation land preceding the anemometer inline with the MetStation and the PNWWF. A surface roughness of 0.1 is given for AG. The Shaniko MetStation is on a high elevation plateau and a value of 0.1 is given for $z_0$. The MetStation of Roosevelt is on a high ridge above the Columbia gorge and a surface roughness of 0.1 is assigned.

Table 2.3: BPA MetStations Wind Speed Scale Factor

| | Tower (ft) | Tower (m) | $z_0$ | $\alpha_s$ | Scale Factor |
|---|---|---|---|---|---|
| AG | 70 | 21.336 | 0.1 | 0.1711 | 1.254 |
| HR | 30 | 9.144 | 0.4 | 0.2674 | 1.786 |
| SH | 30 | 9.144 | 0.1 | 0.2026 | 1.552 |
| RV | 70 | 21.336 | 0.1 | 0.1711 | 1.254 |

The scale factors in Table 2.3 were applied to the wind speed time series data sets before being used by any of the models discussed below.

## 2.6 Wind Direction

Once the angle and degree of acceptance for the digital direction indicators were established, a wind direction survey was run on the BPA data. The percentage in Table 2.4 refers to the ratio of the number of times the correct wind direction was detected to the total number of samples. The results in Table 2.4 reveal some interesting directional behavior. Cases 5 through 10 indicate that the wind blowing toward the PNWWF is coming from almost opposite directions. This is probably not felt at the wind farm, most of the time, as there is some meteorological mechanism at work that channels air in one direction.

Table 2.4: Wind Direction Survey Results

| Case | Blowing towards PNWWF | Percentage |
|---|---|---|
| 1 | AG | 60 |
| 2 | HR | 73 |
| 3 | SH | 18 |
| 4 | RV | 30 |
| 5 | AG and HR | 52 |
| 6 | AG and RV | 6 |
| 7 | AG and SH | 6 |
| 8 | HR and RV | 14 |
| 9 | RV and SH | 8 |
| 10 | AG, HR, SH, and RV | 1 |
| 11 | AG, HR, SH, and RV are NOT blowing towards PNWWF | 2 |

Since wind direction was not captured for the PNWWF it is not possible to resolve the contribution of the wind direction combinations in cases 6 – 11; therefore these cases will not be considered in the ARMA model. There is one exception to the previous statement. The proximity of Augspurger and Hood River, Table 2.4, case 5, suggest that it is reasonable to include that specific combination in one of the models.

## 3 Wind Speed Prediction

Several models were developed and tested in the process of trying to find the best performing model. In order to simplify reference to each model they will be named in order of introduction. Wind samples are designated $W_{WF}(k)$ for wind farm or $W_{MS}(k)$ for wind data from a BPA meteorological station. The order of filter, p, is the number of samples used in the prediction calculation starting from the current sample, W(k), to the filters length W(k-p). Subscripts are added to distinguish wind farm samples from MetStation samples (e.g. $p_{WF}$ or $p_{MS}$). The length of the horizon being estimated is $N_H$, and the number of training samples is $N_T$. The number of training samples must always be larger than the combined number of filter samples used in coefficient training. To ensure this relationship is not violated the MATLAB code will check and will return an error if the length constraint is violated.

In this research there is Model 0, which is an autoregression model. Additionally, there are three ARMA models, named Model 1, 2 and 3.

In general, all of the models operated on the time series data using a sliding window starting at the most recent sample, W(k). Model 2 introduces a small exception to this generality. In all of the models the filter order will refer to the number of samples from the time series being used for prediction. With the exception of Model 0, the filter order for the wind farm is equal to the filter size representing the BPA meteorological stations.

## 3.1 Model Training

Training refers to the computation of the coefficients or weights for the system. Training length will be discussed in section 3.1.2.

### 3.1.1 Coefficient Generation

The general case for the prediction model is **Y**=**XB** where **Y** and **B** are column vectors and **X** is a rectangular matrix with m rows always greater than n columns. To generate the coefficients, the **B** matrix, must be solved for by the following equation (4) [14].

$$
\begin{aligned}
&Y = XB \\
&X^{-1}Y = B && \text{; if X is a square matrix} \\
&\left(X^T X\right)^{-1} X^T Y = B && \text{; if X is rectangular}
\end{aligned}
\tag{4}
$$

**X** is an, m x n rectangular matrix where m and n are defined by the following:

m = training length

n = filter order

Since the number of training samples is always constrained to be larger than the filter order, the pseudo-inverse [14] in equation (4) will be used.

### 3.1.2 Training Length

The training length represents the past history of the time series and should be of sufficient length to capture diurnal patterns temporally localized to a particular season. If the training length is too short approaching the filter order or number of estimated horizons then the predictions become unstable (overshoot and undershoot) in ramp events. To illustrate this behavior Model 0 was run with a training length of 144 samples (one day). The red trace is the prediction that overshoots. A view of the complete data set is plotted in Figure 3.2 and large instabilities (red) are readily apparent along with negative wind velocities that are also generated.

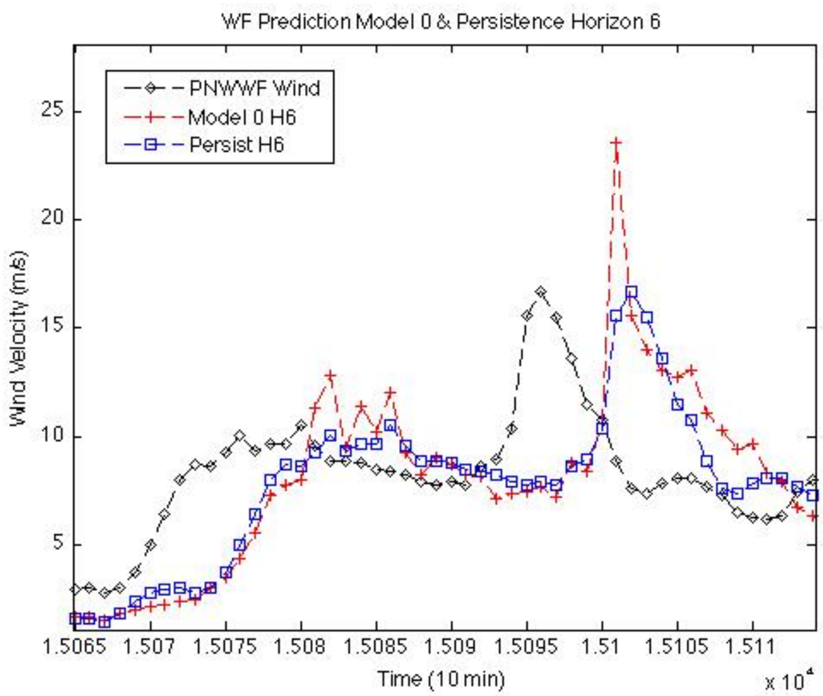


Figure 3.1:Model 0, Train 144

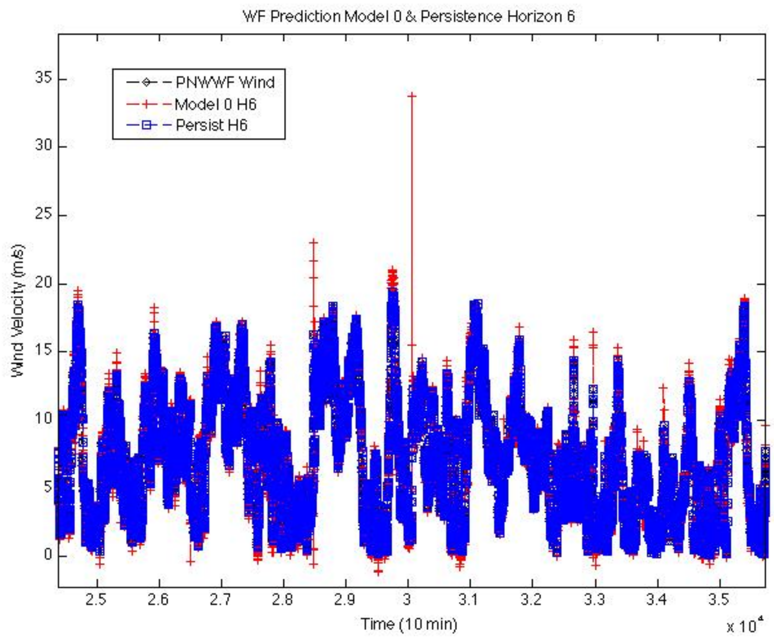


Figure 3.2: Model 0, Train 144, Longer Time Interval

A very long training period is not desired as seasonal effects change the wind profile and thus the results would have more error. The weights are a least mean squares fit [15] of the training set. As the training length grows longer the coefficients will start to lose distinguishing patterns such as diurnal variations and wind ramps. Figure 3.3 through Figure 3.5 illustrate the effect of training length on the behavior of the predictions. All three plots used Model 0 with the same filter order and prediction horizon throughout each figure.

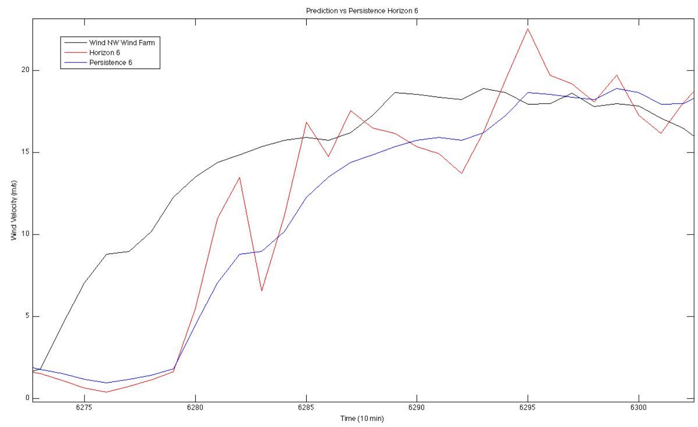


Figure 3.3: Model 0, Train 144

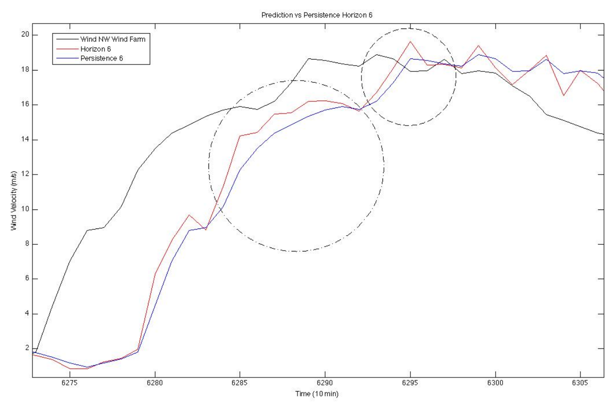


Figure 3.4:Model 0 Train 1728

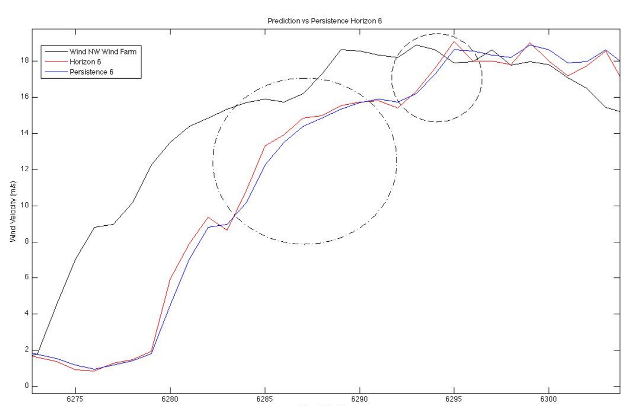


Figure 3.5: Model 0 Train 5760

### 3.1.3 Filter Order

Where the training length captures the characteristics of the wind velocity over a long period of time the filter order has a much shorter length (5 to 20 samples) and represents the present conditions in the time series. The process of determining the filter order will be discussed next. Revisiting Table 2.1 it is noticed that, while the distance from the Roosevelt MetStation to the wind farm is 35km the distance from the other three MetStations to the wind farm is in the 70-80 km range. Roughly there is a 2:1 ratio of distance between the wind farm and Augspurger, Hood River, and Shaniko as compared to the wind farm to Roosevelt distance. It is reasonable to expect the filter order of AG, HR, and SH to be twice the filter order of RV. With this constraint the MATLAB program computed increasing filter orders and recorded the mean squared error. Table 3.1 list the filter order based upon the minimum MSE.

Table 3.1: Model 1, 2, 3 Characteristics

| BPA MS | Filter Order | Training Length |
|---|---|---|
| Augspurger (AG) | 10 | 1728 |
| Hood River (HR) | 10 | 1728 |
| Shaniko (SH) | 10 | 1728 |
| Roosevelt (RV) | 5 | 1728 |

## 3.2 AR and ARMA Models

In examining the performance of the models developed during this research the mean squared error was computed for each horizon and will be presented. However, the MSE only gives a general indication of performance and does not differentiate from wind ramp events, slowly changing wind speeds, or steady state wind speed. To get a better picture of performance plots of an extreme wind ramp event and a medium wind ramp event will be included to illustrate how each model performs during ramp events. The plot an extreme wind ramp along with the power ramp is shown in Figure 3.6, and a medium wind ramp and power ramp event is shown in Figure 3.7. The extreme wind ramp was found by searching the time series for the greatest m/s/hour change. The extreme ramp event is interesting because it leads to a high-speed cutout event that produces a large downward ramp. This event is similar to an event in the Electricity Reliability Council of Texas (ERCOT) system on February 24, 2007. The power down ramp event was a result of wind farms in west Texas shutting down due to excessive wind speed that exceeded the turbines cutout speed. Unfortunately, this event occurred at 9:00 am when the system load was increasing exacerbating the imbalance.

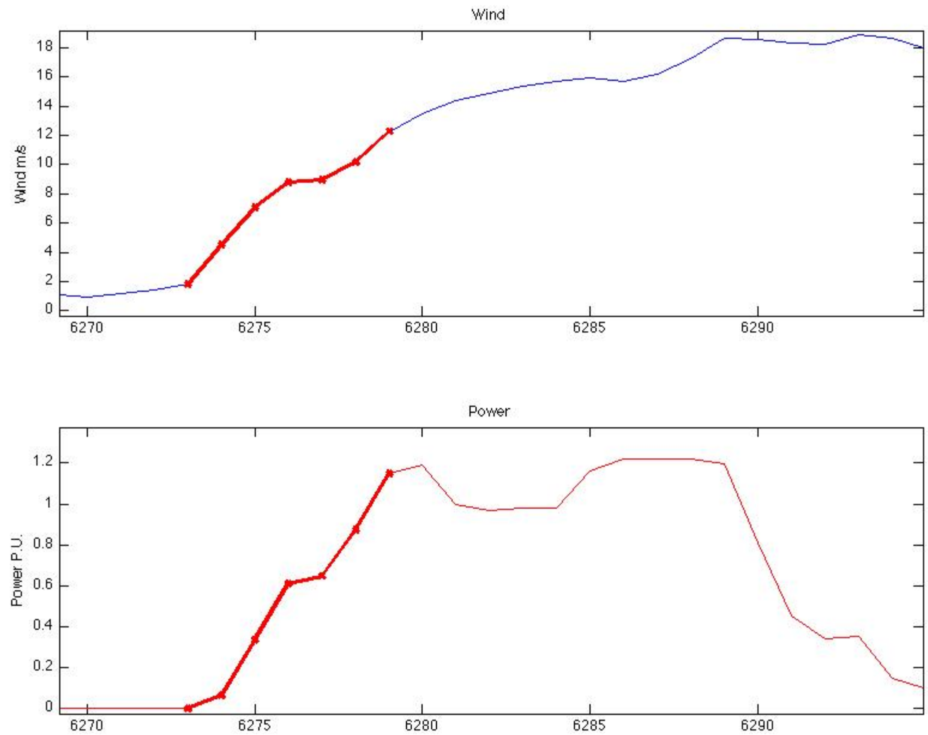


Figure 3.6: Extreme Wind Ramp Event

The extreme wind ramp event has a wind speed change of 10.5 m/s/hr in the red section, and a power ramp of 113 MW/hr. The extreme ramp event is followed by what appears to be a shut down of the turbines due to high wind speeds. The manufacture's data sheet for this model turbine list the 10-minute cutout wind speed at 20 m/s. The peak wind speed in Figure 3.6 is 18.6 m/s when the power suddenly drops. The wind speed in Figure 3.6 is the average wind velocity across the entire wind farm. Judging by the shape of the power ramp some turbines are still in operation while the turbines in the faster moving air have shut down.  The medium ramp event has a wind speed change of 6.1 m/s/hr and a power ramp of 85MW/hr.

The plots selected are upward ramps and shown to illustrate performance, but it should be noted that downward ramps exhibit the same performance. Also, the plots selected demonstrate good performance of the ARMA filter, but there are many wind ramps that didn't show any noticeable improvement over the persistence model.

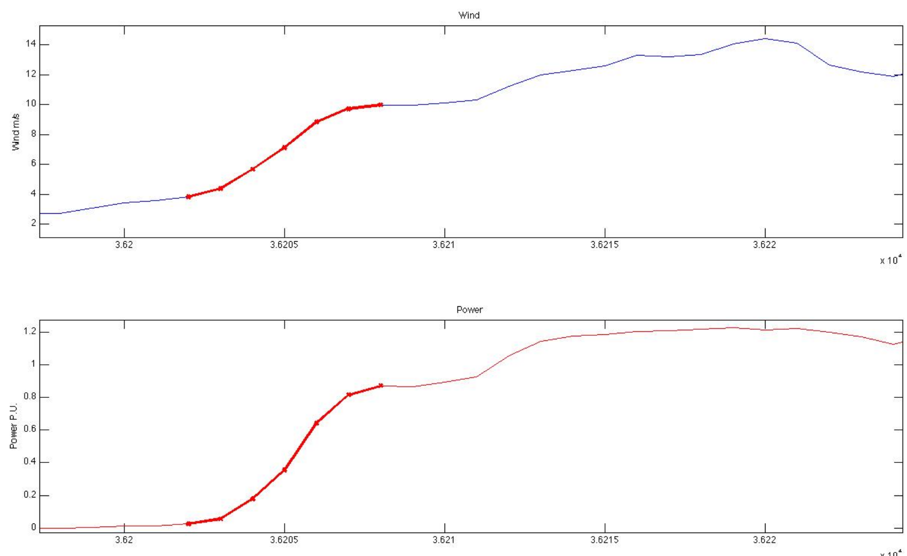


Figure 3.7: Medium Wind Ramp Event

## 3.3 Model 0

Model 0 is based on an autoregressive (AR) mathematical model, and the equation for prediction is shown (5). The filter size for this model represents then number of samples used for prediction. The estimate, $W_{WF}(k+2)$, relies on the previous estimate, $W_{WF}(k+1)$, being computed before computation of $W_{WF}(k+2)$ can proceed. The same restriction applies to estimates, $W_{WF}(k+3)$ through $W_{WF}(k+N_H)$.

$$\begin{bmatrix} W_{WF}(k+1) \\ W_{WF}(k+2) \\ \vdots \\ W_{WF}(k+N_H) \end{bmatrix} = \begin{bmatrix} W_{WF}(k) & W_{WF}(k-1) & \dots & W_{WF}(k-p_{WF}) \\ W_{WF}(k+1) & W_{WF}(k) & \dots & W_{WF}(k+1-p_{WF}) \\ \vdots & \vdots & \ddots & \vdots \\ W_{WF}(k+N_H-1) & W_{WF}(k+N_H-2) & \cdots & W_{WF}(k+N_H-1-p_{WF}) \end{bmatrix} \begin{bmatrix} \alpha_1 \\ \alpha_2 \\ \vdots \\ \alpha_{p_{WF}} \end{bmatrix} \quad (5)$$

$$\begin{bmatrix} W_{WF}(k) \\ W_{WF}(k-1) \\ \vdots \\ W_{WF}(k-N_T) \end{bmatrix} = \begin{bmatrix} W_{WF}(k-1) & W_{WF}(k-2) & \dots & W_{WF}(k-1-p_{WF}) \\ W_{WF}(k-2) & W_{WF}(k-3) & \dots & W_{WF}(k-2-p_{WF}) \\ \vdots & \vdots & \ddots & \vdots \\ W_{WF}(k-N_T-1) & W_{WF}(k-N_T-2) & \cdots & W_{WF}(k-N_T-1-p_{WF}) \end{bmatrix} \begin{bmatrix} \alpha_1 \\ \alpha_2 \\ \vdots \\ \alpha_{p_{WF}} \end{bmatrix} \quad (6)$$

The coefficients for the B column vector are generated using equation (6).

### 3.3.1 Model 0 Results

To determine a reasonable filter length the training length was held constant at 1728 samples (6 days) and the filter order was varied from 2 to 20. A filter length of 10 was selected for Model 0 and the mean squared error (MSE) results indicate an improvement over the persistence model.

Table 3.2: MSE Model 0

| Horizon | MSE PM | MSE Model 0 |
|---|---|---|
| 1 | 0.0151 | 0.0123 |
| 2 | 0.0426 | 0.0395 |
| 3 | 0.0708 | 0.0680 |
| 4 | 0.0981 | 0.0954 |
| 5 | 0.1248 | 0.1221 |
| 6 | 0.1510 | 0.1479 |
| 7 | 0.1769 | 0.1733 |
| 8 | 0.2024 | 0.1984 |
| 9 | 0.2277 | 0.2232 |
| 10 | 0.2527 | 0.2473 |
| 11 | 0.2776 | 0.2715 |
| 12 | 0.3029 | 0.2959 |

Although the MSE indicates better performance examination of the time series plot in Figure 3.8 shows that in a medium type ramp event Model 0 offers a small improvement over the persistence model. Examination of the extreme ramp event, Figure 3.9, shows that Model 0 is performing marginally better than the persistence model.

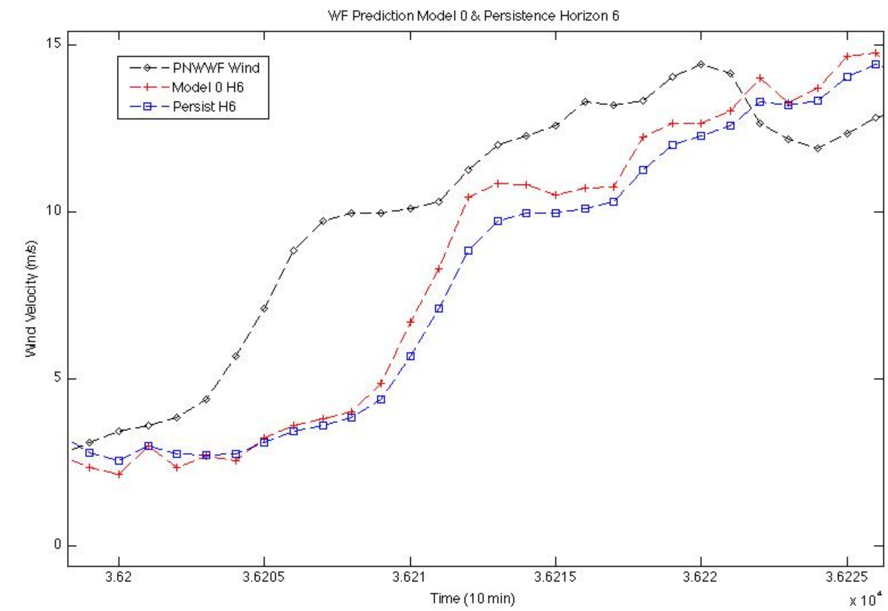


Figure 3.8: Model 0, Horizon 6, Medium Ramp Event

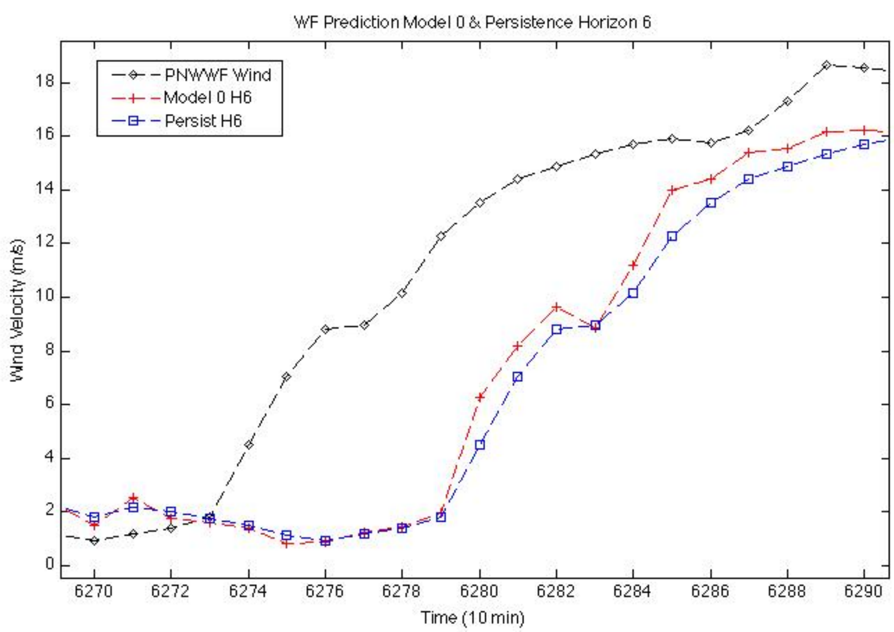


Figure 3.9: Model 0 Horizon 6 Extreme Ramp Event

## 3.4 Model 1

Model 1 is an ARMA model that uses the BPA meteorological sites as the moving average portion of the model. The **X** in prediction matrix, **Y**=**XB**, is made up of time series samples from the wind farm and the MetStations. The matrix **X** is a horizontal concatenation of $\mathbf{X_{WF}}$ and $\mathbf{X_{MS}}$. In MATLAB code it would be expressed as the following:

$$X = [X_{WF}\ X_{MS}] \tag{7}$$

$\mathbf{X_{WF}}$ & $\mathbf{X_{MS}}$ are matrices, not necessarily square, with m rows set by the number of horizons desired, and n columns determined by the filter order.

The prediction computation for Model 1 is shown in (8). Remembering that $N_H$ is the maximum number of predictions, the computation of $W_{WF}(k+2)$ through $W_{WF}(k+N_H)$ all rely upon the previous estimate being generated before inclusion into the current estimate computation.

$$\begin{bmatrix} W_{WF}(k+1) \\ W_{WF}(k+2) \\ \vdots \\ W_{WF}(k+N_H) \end{bmatrix} = \begin{bmatrix} W_{WF}(k) & W_{WF}(k-1) & \dots & W_{WF}(k-p_{WF}) & W_{MS}(k) & W_{MS}(k-1) & \cdots & W_{MS}(k-p_{MS}) \\ W_{WF}(k+1) & W_{WF}(k) & \dots & W_{WF}(k+1-p_{WF}) & W_{MS}(k+1) & W_{MS}(k) & \cdots & W_{MS}(k+1-p_{MS}) \\ \vdots & \vdots & \ddots & \vdots & \vdots & \vdots & \ddots & \vdots \\ W_{WF}(k+N_H-1) & W_{WF}(k+N_H-2) & \cdots & W_{WF}(k+N_H-1-p_{WF}) & W_{MS}(k+N_H-1) & W_{MS}(k+N_H-2) & \cdots & W_{MS}(k+N_H-1-p_{MS}) \end{bmatrix} \begin{bmatrix} \alpha_1 \\ \alpha_2 \\ \vdots \\ \alpha p_{WF} \\ \beta_1 \\ \beta_2 \\ \vdots \\ \beta p_{MS} \end{bmatrix} \tag{8}$$

Model 1 also requires use of the intermediate predicted variables, $W_{MS}(k+1)$ through $W_{MS}(k+N_H-1)$, in the computation of $W_{WF}(k+2)$ through $W_{WF}(k+N_H)$, and those intermediate predicted variables are generated by the equation shown in equation (9).

$$\begin{bmatrix} W_{MS}(k+1) \\ W_{MS}(k+2) \\ \vdots \\ W_{MS}(k+N_H) \end{bmatrix} = \begin{bmatrix} W_{MS}(k) & W_{MS}(k-1) & \dots & W_{MS}(k-p_{MS}) \\ W_{MS}(k+1) & W_{MS}(k) & \dots & W_{MS}(k+1-p_{MS}) \\ \vdots & \vdots & \ddots & \vdots \\ W_{MS}(k+N_H-1) & W_{MS}(k+N_H-2) & \cdots & W_{MS}(k+N_H-1-p_{MS}) \end{bmatrix} \begin{bmatrix} \zeta_1 \\ \zeta_2 \\ \vdots \\ \zeta p_{MS} \end{bmatrix} \quad (9)$$

The ζ coefficients are generated using a training set from the BPA meteorological station time series. The training equations are shown in equation (10. Each BPA meteorological station has a unique set of coefficients generated from the training size filter order for a particular MetStation. The ζ weight generation is performed once per new wind farm data sample.

$$\begin{bmatrix} W_{MS}(k) \\ W_{MS}(k-1) \\ \vdots \\ W_{MS}(k-Nt) \end{bmatrix} = \begin{bmatrix} W_{MS}(k-1) & W_{MS}(k-2) & \dots & W_{MS}(k-1-p_{MS}) \\ W_{MS}(k-2) & W_{MS}(k) & \dots & W_{MS}(k-2-p_{MS}) \\ \vdots & \vdots & \ddots & \vdots \\ W_{MS}(k-Nt-1) & W_{MS}(k-Nt-2) & \cdots & W_{MS}(k-Nt-1-p_{MS}) \end{bmatrix} \begin{bmatrix} \zeta_1 \\ \zeta_2 \\ \vdots \\ \zeta p_{MS} \end{bmatrix} \quad (10)$$

The α and β coefficients are generated by solving the equation (11) for the **B** column vector.

$$\begin{bmatrix} W_{WF}(k) \\ W_{WF}(k-1) \\ \vdots \\ W_{WF}(k-Nt) \end{bmatrix} = \begin{bmatrix} W_{WF}(k-1) & W_{WF}(k-2) & \dots & W_{WF}(k-1-p_{WF}) & W_{MS}(k-1) & W_{MS}(k-2) & \cdots & W_{MS}(k-1-p_{MS}) \\ W_{WF}(k-2) & W_{WF}(k-3) & \dots & W_{WF}(k-2-p_{WF}) & W_{MS}(k-2) & W_{MS}(k-3) & \cdots & W_{MS}(k-2-p_{MS}) \\ \vdots & \vdots & \ddots & \vdots & \vdots & \vdots & \ddots & \vdots \\ W_{WF}(k-Nt-1) & W_{WF}(k-Nt-2) & \cdots & W_{WF}(k-Nt-1-p_{WF}) & W_{MS}(k-Nt-1) & W_{MS}(k-Nt-2) & \cdots & W_{MS}(k-Nt-1-p_{MS}) \end{bmatrix} \begin{bmatrix} \alpha_1 \\ \alpha_2 \\ \vdots \\ \alpha p_{WF} \\ \beta_1 \\ \beta_2 \\ \vdots \\ \beta p_{MS} \end{bmatrix} \quad (11)$$

The size of the training set is constrained, in the program code, to ensure that it is always greater than twice the size of the filter order for the BPA MetStation being used in the prediction. The training set consists of samples from the wind farm and meteorological station time series.

### 3.4.1 Model 1 Results

As seen in Table 2.4 there is fair percentage of time that the wind is blowing towards the PNWWF from multiple MetStations. The four BPA meteorological stations provided wind direction data, but the PNWWF data set did not have wind direction included. Therefore a priority had to be assigned in the case of multiple MetStations indicating a valid wind direction. This priority for Model 1 is Augspurger, Hood River, Shaniko and Roosevelt. To investigate if the wind from Hood River, Roosevelt or Shaniko had an influence on the performance, Model 1A, Model 1B, and Model 1C were created to change the priority to different MetStations. Model 1A gave priority in the following descending order: Hood River, Augspurger, Shaniko, and Roosevelt. The priority, in descending order, for Model 1B was the following: Roosevelt, Augspurger, Hood River, and Shaniko. The descending order priority for Model 1C was Shaniko, Augspurger, Hood River, and Roosevelt.

Based on the filter order in 3.1.3 the MSE was computed for each horizon and listed Table 3.3.

Table 3.3: MSE Model 1

| Horizon | PM | Model 1 | Model 1A | Model 1B | Model 1C |
|---|---|---|---|---|---|
| 1 | 0.0151 | 0.0123 | 0.0124 | 0.0124 | 0.0124 |
| 2 | 0.0426 | 0.0393 | 0.0394 | 0.0394 | 0.0395 |
| 3 | 0.0708 | 0.0668 | 0.0672 | 0.0672 | 0.0673 |
| 4 | 0.0981 | 0.0927 | 0.0934 | 0.0934 | 0.0935 |
| 5 | 0.1248 | 0.1172 | 0.1183 | 0.1184 | 0.1183 |
| 6 | 0.1510 | 0.1404 | 0.1421 | 0.1421 | 0.1419 |
| 7 | 0.1769 | 0.1627 | 0.1653 | 0.1649 | 0.1647 |
| 8 | 0.2024 | 0.1843 | 0.1879 | 0.1870 | 0.1867 |
| 9 | 0.2277 | 0.2053 | 0.2102 | 0.2086 | 0.2083 |
| 10 | 0.2527 | 0.2256 | 0.2317 | 0.2296 | 0.2290 |
| 11 | 0.2776 | 0.2457 | 0.2531 | 0.2506 | 0.2495 |
| 12 | 0.3029 | 0.2660 | 0.2744 | 0.2717 | 0.2702 |

The MSE results indicate that Model 1 is performing better than the other three models, but this is probably because there is a good deal of wind blowing from AG and HR towards the wind farm and the MetStation at AG is less obstructed than the HR station.

The plot results for horizon 6, Figure 3.10, shows an improvement over the persistence model for the medium ramp case. Bold red dots are placed at one-hour separations. The predicted wind speed for Model 1 is well within the boundary set by the persistence model. As the ramp event starts to form, Model 1 is marginally better than the PM, but as the ramp progresses the prediction by Model 1 improves considerably. The transitional areas, local maxima or minima, appear to be a weakness in the model, as the prediction does not track any better than the persistence model at points of inflection. With a smaller training length this weakness becomes more apparent as was demonstrated earlier in the discussion of training length.

In the extreme ramp case, Model 1 starts predicting the upward ramp earlier, Figure 3.11, than for the medium ramp and well within the boundary of the persistence model. The third hour prediction (red line), made at hour 2, is remarkably accurate.

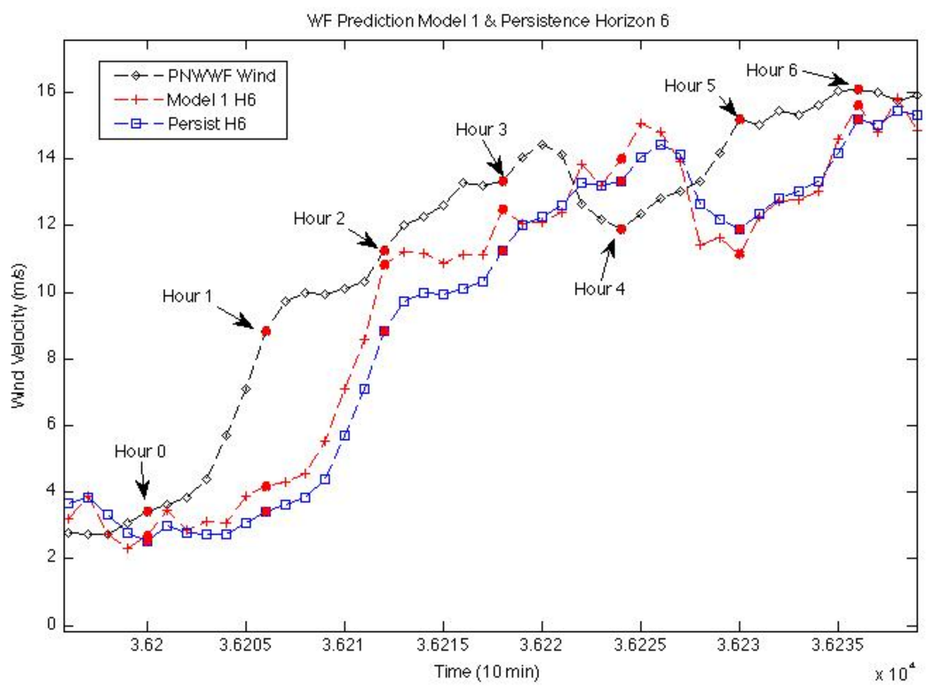


Figure 3.10: Model 1, Horizon 6, Medium Ramp Event

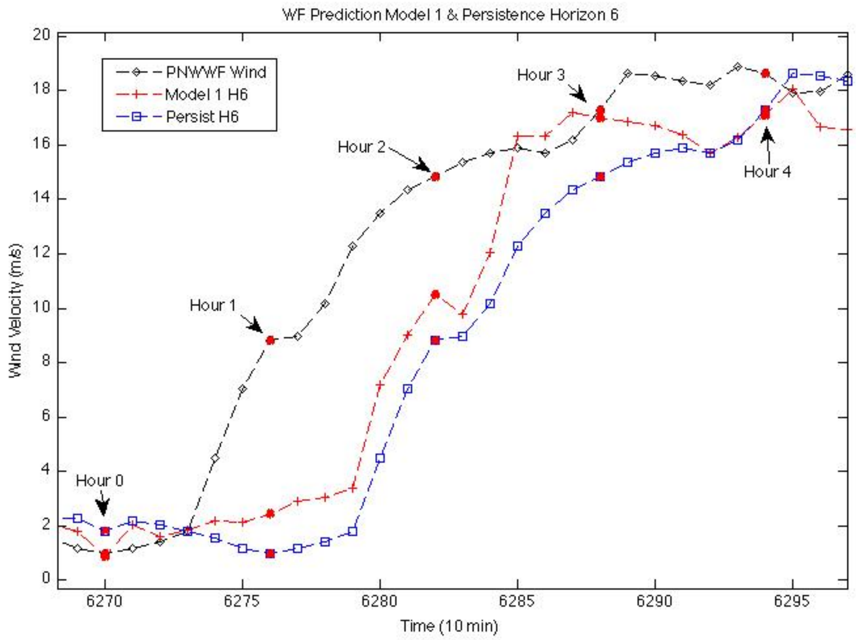


Figure 3.11:Model 1, Horizon 6, Extreme Ramp Event

Comparing the medium ramp and the extreme ramp, it is noticed that both cases the model prediction accuracy improves by the second hour. The wind direction during the extreme ramp was coming from Augspurger and Roosevelt.

## 3.5 Model 2

All of the intermediate prediction values in Model 1, equation (12) were computed estimates. As in Model 1, the matrix **X** is a horizontal concatenation of $\mathbf{X_{WF}}$ and $\mathbf{X_{MS}}$. If there is error in the predicted values, $W_{MS}(k+1)$ through $W_{MS}(k+N_H)$, then that error would be incorporated into the wind farm's **X** matrix. Instead of predicting the intermediate values for $W_{MS}(k+1)$ through $W_{MS}(k+N_H)$, the time series samples for these variables will be offset by the maximum estimate (e.g. $W_{MS}(k-N_H)$) as shown in the prediction equation (12). For each horizon prediction, the intermediate values would be progressing toward the current sample, W(k) using real values for the prediction instead of computed values.

$$\begin{bmatrix} W_{WF}(k+1) \\ W_{WF}(k+2) \\ \vdots \\ W_{WF}(k+N_H) \end{bmatrix} = \begin{bmatrix} W_{WF}(k) & W_{WF}(k-1) & \ldots & W_{WF}(k-p_{WF}) & W_{MS}(k-N_H) & W_{MS}(k-N_H-1) & \cdots & W_{MS}(k-N_H-p_{MS}) \\ W_{WF}(k+1) & W_{WF}(k) & \ldots & W_{WF}(k-p_{WF}+1) & W_{MS}(k-N_H+1) & W_{MS}(k) & \cdots & W_{MS}(k-N_H-p_{MS}+1) \\ \vdots & \vdots & \ddots & \vdots & \vdots & \vdots & \ddots & \vdots \\ W_{WF}(k+Np-1) & W_{WF}(k+Np-2) & \cdots & W_{WF}(k) & W_{MS}(k) & W_{MS}(k-1) & \cdots & W_{MS}(k-p_{MS}) \end{bmatrix} \begin{bmatrix} \alpha_1 \\ \alpha_2 \\ \vdots \\ \alpha p_{BL} \\ \beta_1 \\ \beta_2 \\ \vdots \\ \beta p_{MS} \end{bmatrix} \quad (12)$$

The training model in equation (13) has an offset of $W_{MS}(k-N_H-1)$ for time series samples for the MetStations.

$$\begin{bmatrix} W_{WF}(k) \\ W_{WF}(k-1) \\ \vdots \\ W_{WF}(k-N_T) \end{bmatrix} = \begin{bmatrix} W_{WF}(k-1) & W_{WF}(k-2) & \ldots & W_{WF}(k-p_{WF}) & W_{MS1}(k-N_H-1) & W_{MS1}(k-N_H-2) & \cdots & W_{MS1}(k-N_H-1-p_{MS1}) \\ W_{WF}(k-2) & W_{WF}(k-3) & \ldots & W_{WF}(k-p_{WF}-1) & W_{MS1}(k-N_H-2) & W_{MS1}(k-N_H-3) & \cdots & W_{MS1}(k-N_H-2-p_{MS1}) \\ \vdots & \vdots & \ddots & \vdots & \vdots & \vdots & \ddots & \vdots \\ W_{WF}(k-N_T-1) & W_{WF}(k-N_T-2) & \cdots & W_{WF}(k-N_T-1-p_{WF}) & W_{MS1}(k-N_H-N_T-1) & W_{MS1}(k-N_H-N_T-1) & \cdots & W_{MS1}(k-N_H-N_T-1-p_{MS1}) \end{bmatrix} \begin{bmatrix} \alpha_1 \\ \alpha_2 \\ \vdots \\ \alpha p_{WF} \\ \beta_1 \\ \beta_2 \\ \vdots \\ \beta p_{MS1} \end{bmatrix} \quad (13)$$

### 3.5.1 Model 2 Results

Since Model 1 investigated different priorities in wind blowing towards the wind farm that process will not be repeated for Model 2 or Model 3. The MSE results listed in Table 3.4 indicates that Model 2 does not perform as well as Model 1. The model is predicting better than the PM for a medium ramp event, Figure 3.12, and looks somewhat similar to Model 1.

Table 3.4: Model 2 MSE

| Horizon | MSE PM | MSE Model 2 | MSE Model 1 |
|---|---|---|---|
| 1 | 0.0151 | 0.0124 | 0.0123 |
| 2 | 0.0426 | 0.0396 | 0.0393 |
| 3 | 0.0708 | 0.0677 | 0.0668 |
| 4 | 0.0981 | 0.0942 | 0.0927 |
| 5 | 0.1248 | 0.1196 | 0.1172 |
| 6 | 0.1510 | 0.1437 | 0.1404 |
| 7 | 0.1769 | 0.1670 | 0.1627 |
| 8 | 0.2024 | 0.1897 | 0.1843 |
| 9 | 0.2277 | 0.2118 | 0.2053 |
| 10 | 0.2527 | 0.2330 | 0.2256 |
| 11 | 0.2776 | 0.2536 | 0.2457 |
| 12 | 0.3029 | 0.2739 | 0.2660 |

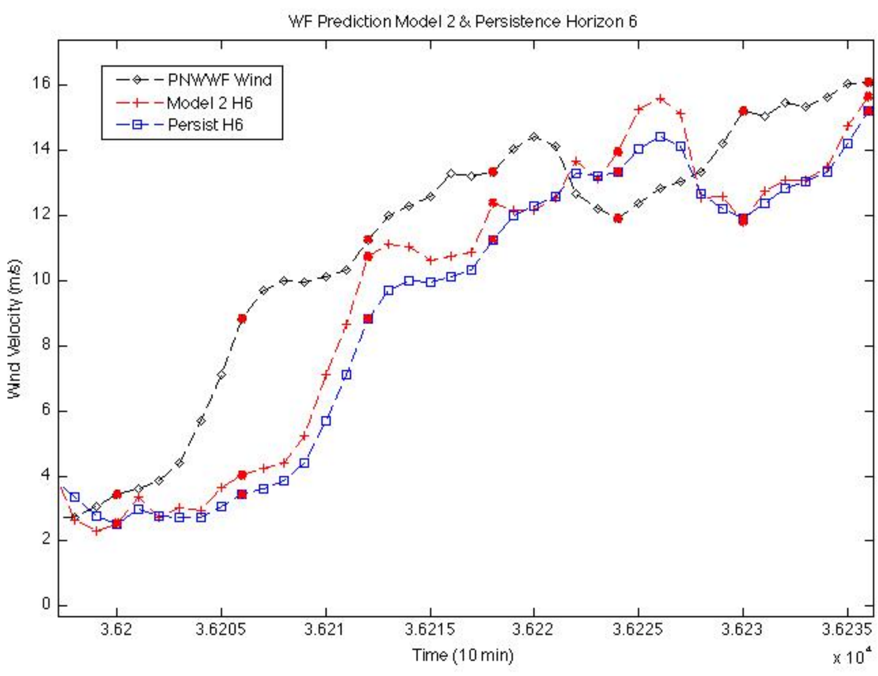


Figure 3.12:Model 2, Horizon 6, Medium Ramp Event

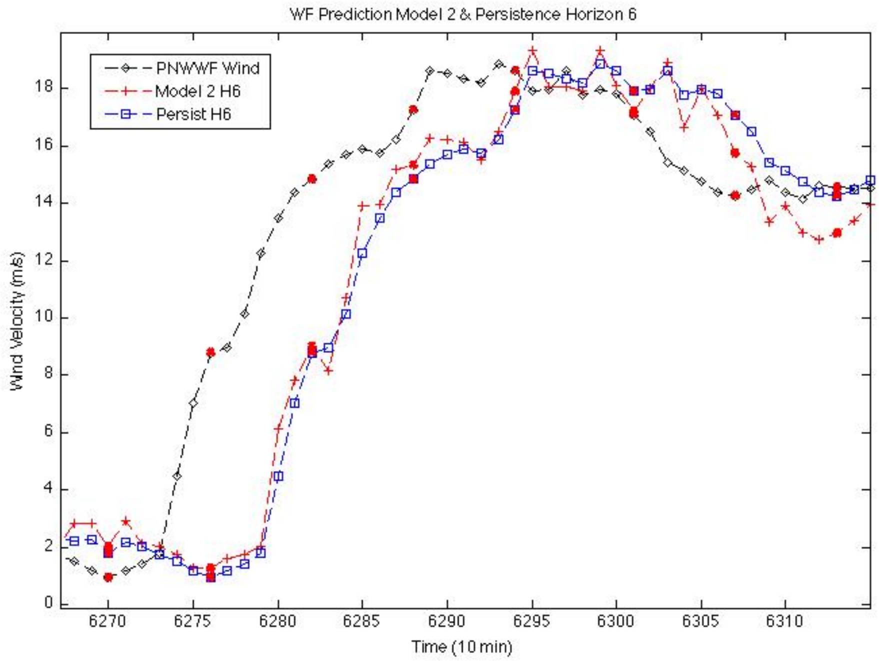


Figure 3.13: Model 2, Horizon 6, Extreme Ramp Event

In the extreme ramp shown in Figure 3.13 there is little difference in prediction between the PM and Model 2event that the most noticeable difference is seen.

## 3.6 Model 3

Model 3 is an extension of the Model 1 ARMA equation. Since Augspurger and Hood River are geographically in the same direction from the wind farm and probably experience the same wind conditions it was reasonable to modify Model 1 to include data from both MetStations when appropriate. The overall prediction equation for the wind farm is given in (15). The **X** in prediction matrix, **Y**=**XB**, is made up of time series samples from the wind farm and two MetStations. The matrix **X** is a horizontal concatenation of $\mathbf{X_{WF}}$, $\mathbf{X_{MS1}}$ and $\mathbf{X_{MS2}}$. In MATLAB code it would be expressed by (14).

$$X = [X_{WF}\ X_{MS1}\ X_{MS2}] \tag{14}$$

$\mathbf{X_{WF}}$, $\mathbf{X_{MS1}}$, and $\mathbf{X_{MS2}}$ are matrices, not necessarily square, with m rows set by the number of horizons desired, and n columns determined by the filter order.

The prediction equation for Model 3 is shown in (15). The computation of $W_{WF}(k+2)$ through $W_{WF}(k+N_H)$ all rely upon the previous estimate being generated before inclusion into the current estimate computation.

$$\begin{bmatrix} W_{WF}(k+1) \\ W_{WF}(k+2) \\ \vdots \\ W_{WF}(k+N_H) \end{bmatrix} = \begin{bmatrix} W_{WF}(k) & W_{WF}(k-1) & \dots & W_{WF}(k-p_{WF}) & W_{MS1}(k) & W_{MS1}(k-1) & \cdots & W_{MS1}(k-p_{MS1}) & W_{MS2}(k) & W_{MS2}(k-1) & \cdots & W_{MS2}(k-p_{MS2}) \\ W_{WF}(k+1) & W_{WF}(k) & \dots & W_{WF}(k+1-p_{WF}) & W_{MS1}(k+1) & W_{MS1}(k) & \cdots & W_{MS1}(k+1-p_{MS1}) & W_{MS2}(k+1) & W_{MS2}(k) & \cdots & W_{MS2}(k+1-p_{MS2}) \\ \vdots & \vdots & \ddots & \vdots & \vdots & \vdots & \ddots & \vdots & \vdots & \vdots & \ddots & \vdots \\ W_{WF}(k+Np-1) & W_{WF}(k+Np-2) & \cdots & W_{WF}(k+Np-p_{WF}) & W_{MS1}(k+Np-1) & W_{MS1}(k+Np-2) & \cdots & W_{MS1}(k+Np-p_{MS1}) & W_{MS2}(k+Np-1) & W_{MS2}(k+Np-2) & \cdots & W_{MS2}(k+Np-p_{MS2}) \end{bmatrix} \begin{bmatrix} \alpha_1 \\ \alpha_2 \\ \vdots \\ \alpha p_{WF} \\ \beta_1 \\ \beta_2 \\ \vdots \\ \beta p_{MS1} \\ \gamma_1 \\ \gamma_2 \\ \vdots \\ \gamma p_{MS2} \end{bmatrix} \quad (15)$$

$$\begin{bmatrix} W_{WF}(k) \\ W_{WF}(k+1) \\ \vdots \\ W_{WF}(k+N_T) \end{bmatrix} = \begin{bmatrix} W_{WF}(k-1) & W_{WF}(k-2) & \cdots & W_{WF}(k-1-p_{WF}) & W_{MS1}(k-1) & W_{MS1}(k-2) & \cdots & W_{MS1}(k-1-p_{MS1}) & W_{MS2}(k-1) & W_{MS2}(k-2) & \cdots & W_{MS2}(k-1-p_{MS2}) \\ W_{WF}(k-2) & W_{WF}(k-3) & \cdots & W_{WF}(k-2-p_{WF}) & W_{MS1}(k-2) & W_{MS1}(k-3) & \cdots & W_{MS1}(k-2-p_{MS1}) & W_{MS2}(k-2) & W_{MS2}(k-3) & \cdots & W_{MS2}(k-2-p_{MS2}) \\ \vdots & \vdots & \ddots & \vdots & \vdots & \vdots & \ddots & \vdots & \vdots & \vdots & \ddots & \vdots \\ W_{WF}(k-N_T-1) & W_{WF}(k-N_T-2) & \cdots & W_{WF}(k-N_T-1-p_{WF}) & W_{MS1}(k-N_T-1) & W_{MS1}(k-N_T-2) & \cdots & W_{MS1}(k-N_T-1-p_{MS1}) & W_{MS2}(k-N_T-1) & W_{MS2}(k-N_T-2) & \cdots & W_{MS2}(k-N_T-1-p_{MS2}) \end{bmatrix} \begin{bmatrix} \alpha_1 \\ \alpha_2 \\ \vdots \\ \alpha p_{WF} \\ \beta_1 \\ \beta_2 \\ \vdots \\ \beta p_{MS1} \\ \gamma_1 \\ \gamma_2 \\ \vdots \\ \gamma p_{MS2} \end{bmatrix} \quad (16)$$

The intermediate prediction results for $W_{MS1}$ and $W_{MS2}$ must be computed as in the same manner as in Model 1. Also the coefficients for producing the intermediate values must be generated and kept separate from the wind farm part of the model.

### 3.6.1 Model 3 Results

The mean squared error for Model 3 gives the appearance that it is performing better than Model 1, but this is not the case. Plotting Model 1 and Model 3 together, there was little improvement --if any-- in upward or downward ramps. The smaller MSE number is probably due to small improvements in small sloped ramps or slowly changing wind as seen in Figure 3.14.

Table 3.5: Model 3 MSE Model 3

| Horizon | MSE PM | MSE Model 3 | MSE Model 1 |
|---|---|---|---|
| 1 | 0.0151 | 0.0123 | 0.0123 |
| 2 | 0.0426 | 0.0393 | 0.0393 |
| 3 | 0.0708 | 0.0668 | 0.0668 |
| 4 | 0.0981 | 0.0925 | 0.0927 |
| 5 | 0.1248 | 0.1169 | 0.1172 |
| 6 | 0.1510 | 0.1399 | 0.1404 |
| 7 | 0.1769 | 0.1619 | 0.1627 |
| 8 | 0.2025 | 0.1832 | 0.1843 |
| 9 | 0.2278 | 0.2039 | 0.2053 |
| 10 | 0.2527 | 0.2240 | 0.2256 |
| 11 | 0.2777 | 0.2439 | 0.2457 |
| 12 | 0.3029 | 0.2640 | 0.2660 |

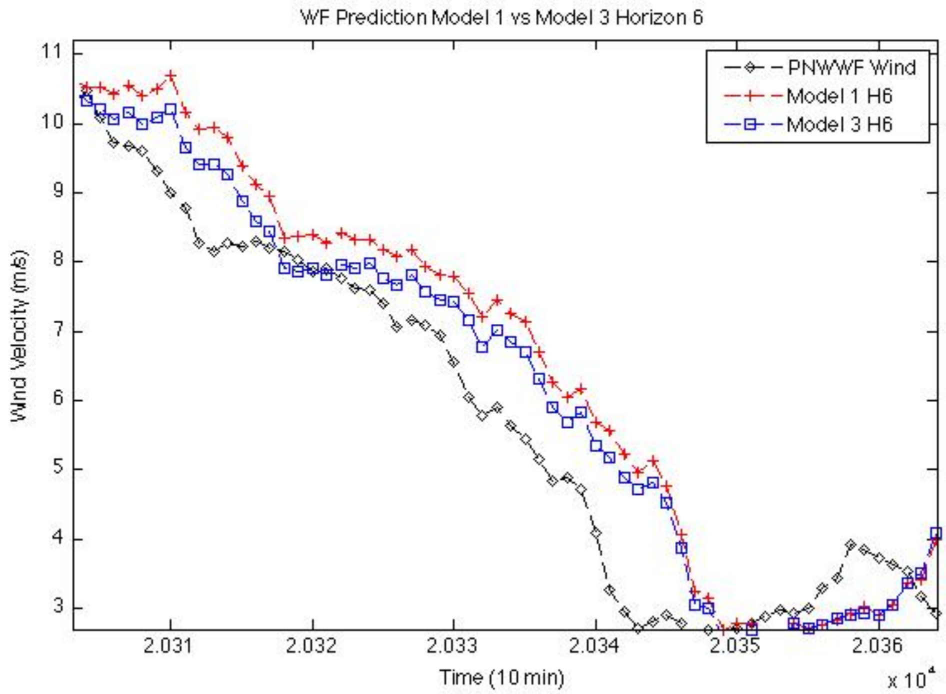


Figure 3.14: Model 1 vs. Model 3

Although this example illustrates Model 3 performing better than Model 1, there are plenty of examples of the opposite case. Manually scanning through the data, situations as in Figure 3.14 probably account for the difference in the MSE values between Model 1 and Model 3. Model 3 does outperform the PM, Figure 3.15 and Figure 3.16, however, it just doesn't offer any advantage over Model 1. The performance of Model 3 would probably improve if wind direction were available at the PNWWF.

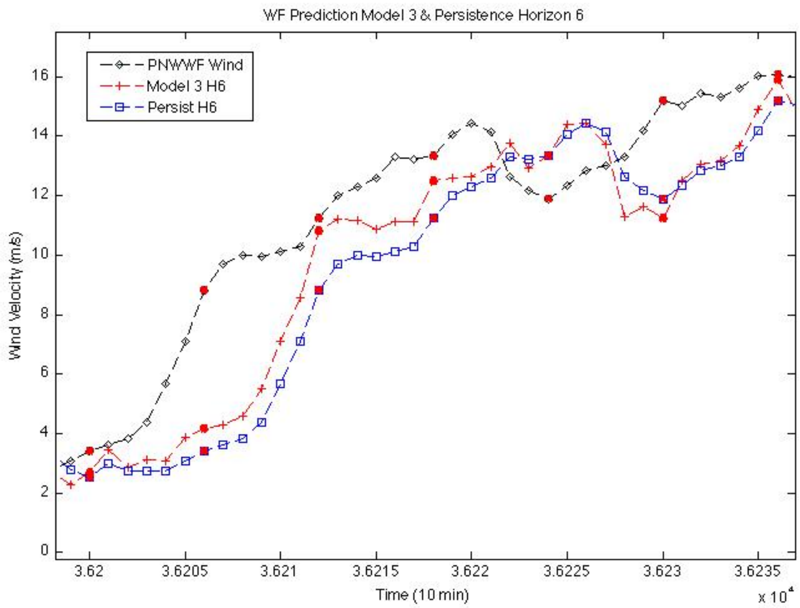


Figure 3.15: Model 3 Medium Ramp Event

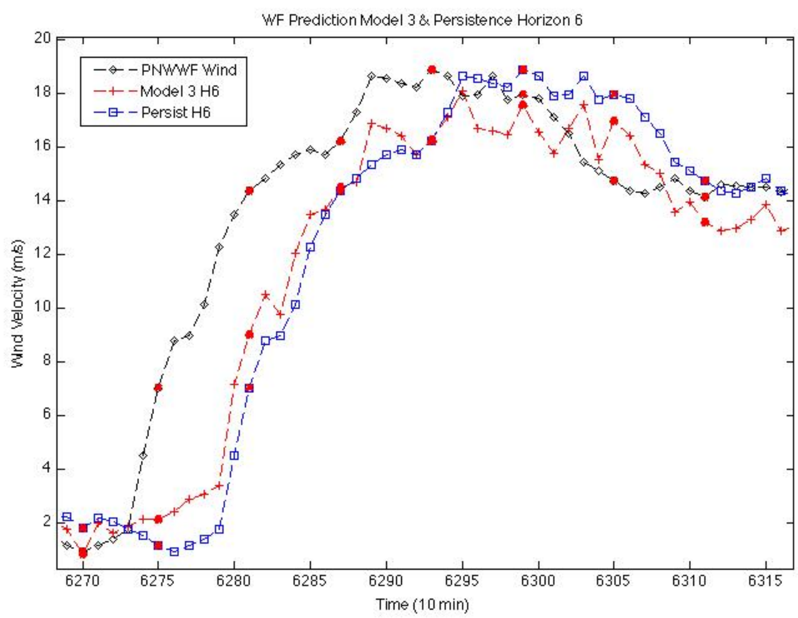


Figure 3.16: Model 3 Extreme Ramp Event

### 3.6.2 Model Conclusions

Model 0 did not perform as well as the other models investigated. It did not have the extra data from the BPA MetStations to influence the computations. Model 2 using actual samples for the intermediate predictions from the MetStations did not perform as well as Model 1. Model 3 demonstrated a little improvement over Model 1, but not in the critical area of upward or downward ramps.

Model 1 investigated using different priorities in the way it handled wind directions coming from more than one MetStation. Looking at the extreme ramp event on the same plot with the wind direction indicators in Figure 3.17 it is seen that AG and HR have wind blowing towards the wind farm during most of the ramp duration. Figure 3.18 plots Model 1 vs. Model 1A and shows a noticeable improvement in the horizon 6 predictions. The improvement is small but noticeable.

For the medium ramp event, wind was blowing towards the wind farm from AG, HR, and SH. The plot of the ramp event, Figure 3.19, shows that the predictions for Model 1 are better than the predictions made by Model 1C.

For any ramp event it was not known which MetStation represented the wind blowing towards the wind farm. The two above cases demonstrate the need for wind direction indication at the PNWWF to provide a more accurate prediction.

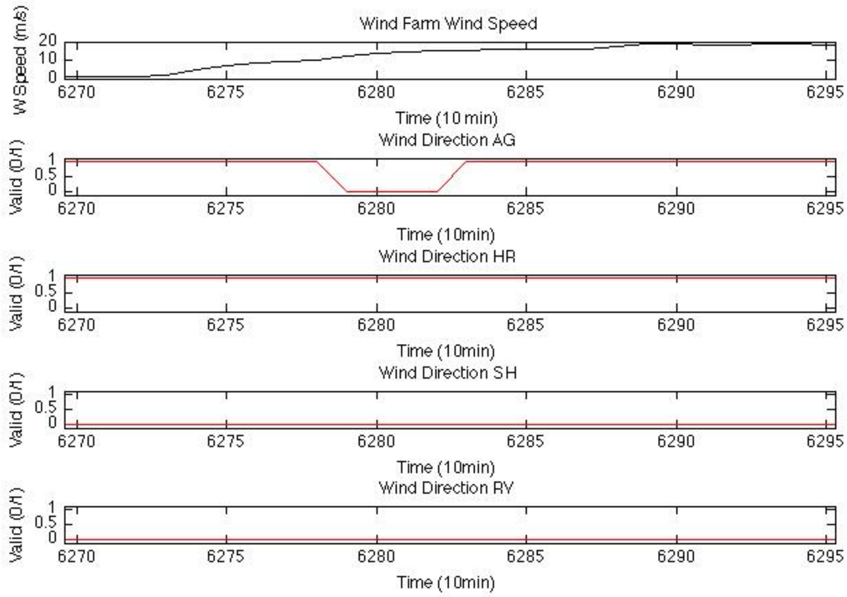


Figure 3.17: Extreme Ramp and Wind Directions

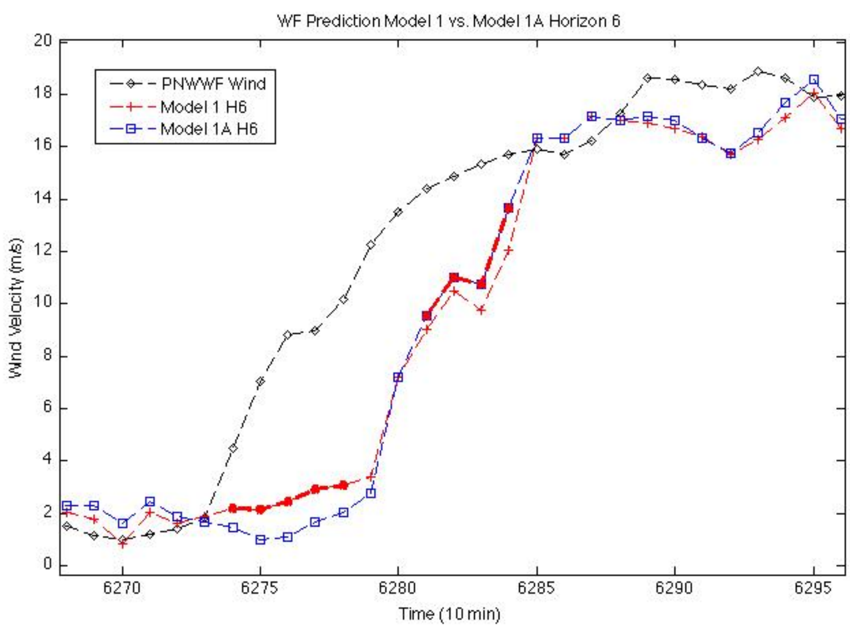


Figure 3.18: Model 1 vs. Model 1A Extreme Ramp Event

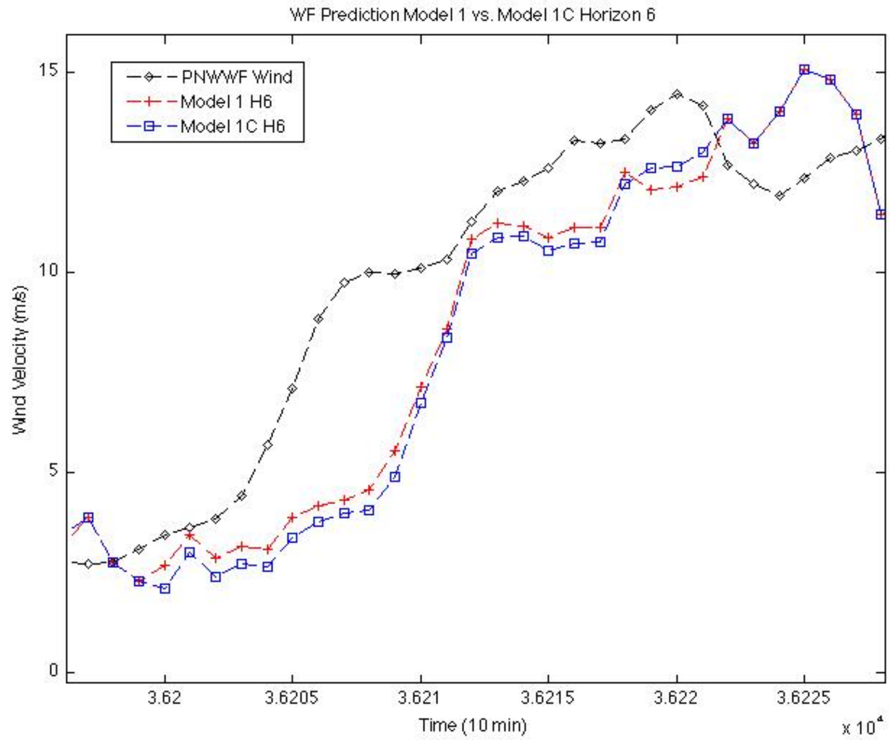


Figure 3.19: Model 1 vs. Model 1C Medium Ramp Event

# 4 Wind Speed to Power Conversion

The wind velocity time series were raw values, not scaled, and averaged across the entire wind farm. Once the wind velocity horizons have been generated then the wind farm power output was computed for each time horizon. The power available in the wind is proportional to the cube of the air velocity, expressed in the (17)[13].

$$P = \frac{1}{2}\rho v^3 \tag{17}$$

The power from the turbine will not follow the equation because wind turbines are non-linear. Using the Vestas power curve [16], Figure 4.1, can be used to convert wind speed to power for each turbine. Multiply the turbine output by the number of active turbines to get the wind farm power output.

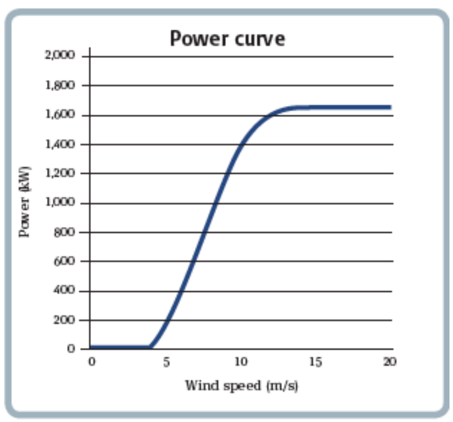


Figure 4.1: Wind Turbine Power Curve

Yen [17] determined that due to the wind velocity variations around a wind farm determining the output is not a straightforward as described above. He then went on to develop a wind farm power curve based upon a statistical analysis of the wind and power output. The MATLAB file from the Yen research was used to compute the wind farm power output horizons based upon the wind speed horizons input.

## 4.1 Wind Power Ramp Profiles

To determine when a power ramp will occur the prediction results, Figure 1.1.1, are used to generate wind farm power output horizons. Model 1A (HR priority over AG) was used to generate the wind speed horizons using a filter order of 10 for Augspurger, Hood River, and Shaniko and five for Roosevelt. Although Model 1 performed better overall, Model 1A performed better during the extreme ramp event. Training length was set at six-days (1728 samples) for all combinations of MetStations and wind farm. The computed plots of power are expressed in P.U. with a 100MW base. The maximum output of the PNWWF is approximately 120MW.

The plots of horizon 6, Figure 4.2, and horizon 12, Figure 4.3, are the computed wind farm power output resulting from the extreme ramp event. The black trace is the actual output --not computed-- from the PNWWF data and is the reference for any horizon. The leading edge of the first ramp is changing at a rate of 1.1MW/hr. The wind prediction had enough accuracy for the Yen [17] power curve model to closely track the actual turbine cutout. The persistence model holds well in accuracy for horizon 6, but in the two-hour projection of horizon 12 the PM suffers performance.

The second large upward power ramp starting at time index 6300, is probably the result of the high wind velocity subsiding a bit and the turbines start producing power again. Here again this is a combination of accurate wind velocity prediction and the wind farm power curve model working together to give this accurate result. Model 1A out performs the PM during the downward slope starting after time index 6320. The mean absolute error for Model 1 and Model 1A were computed and compared with the persistence model shown in Table 4.1.

Table 4.1: MAE Power Prediction

| Horizon | PM | Model 1 | Model 1A |
|---|---|---|---|
| 6 | 0.0709 | 0.0693 | 0.0697 |
| 12 | 0.1017 | 0.0974 | 0.0989 |

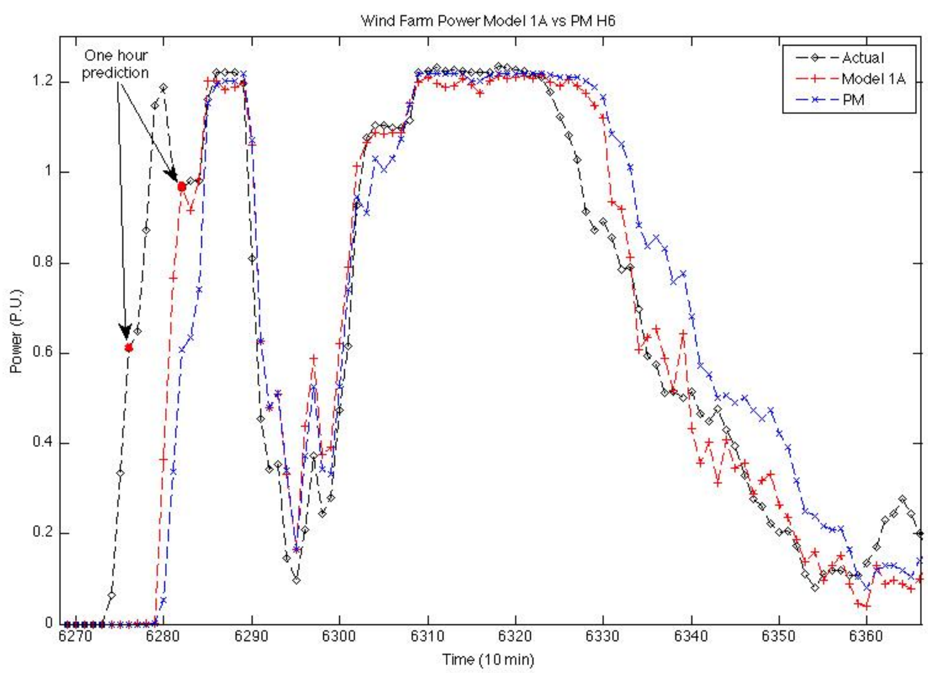


Figure 4.2:Power Prediction, Horizon 6

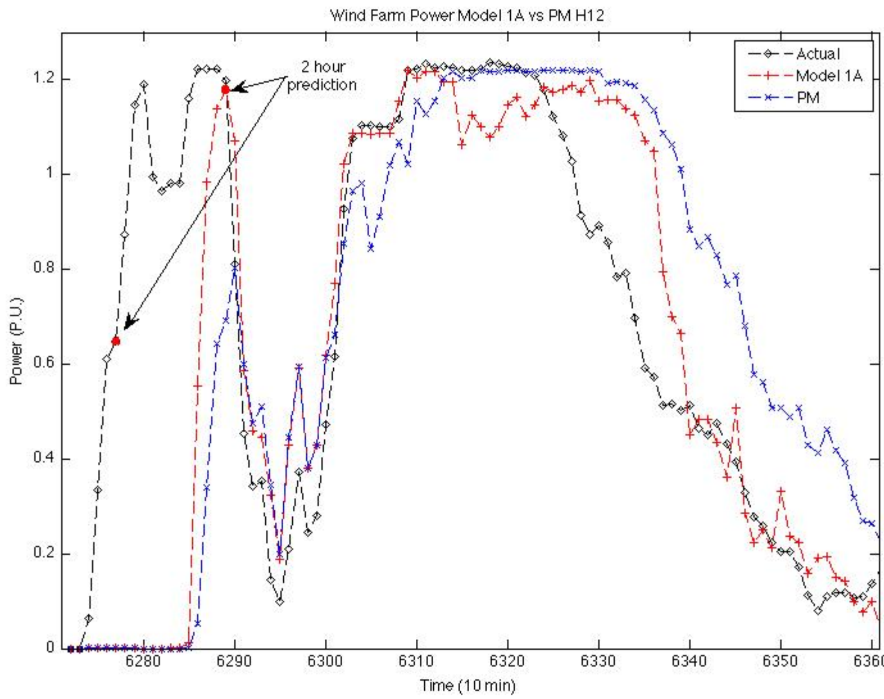


Figure 4.3: Power Prediction, Horizon 12

The MAE results indicate that Model 1 is performing better than Model 1A, which is largely due to wind speed prediction of Model 1 performing better than Model 1A.

## 4.2 Definition: Wind Power Ramp

Wind power ramp definitions try to characterize an increase or decrease in power from a wind farm due to a changing wind condition. Defining a wind ramp seems to be a bit elusive as Klamath [18] points out that there really is not a universal definition. She presented the following definition to address a change in power over an interval.

$$|MW(T + \Delta T) - MW(T)| > Tr \qquad (18)$$

A power ramp is declared if the difference in power is greater than a threshold. However, she goes on to point out that the definition did not address power changes in the interval and consequently set forth a second definition.

$$\max(MW[T+\Delta T]) - \min(MW[T+\Delta T]) > Tr \tag{19}$$

The second definition from Klamath finds the maximum delta MW, but the time difference at the min and max must be known in order to compute the slope and to identify an upward or downward ramp.

The approach by Zheng and Kusiak [19] computed the absolute slope in defining a power ramp rate (PRR).

$$PRR = \frac{|P(T+10) - P(T)|}{10} \tag{20}$$

Where Zheng and Kusiak measured the PRR over 10 minute intervals, the interval could be longer.

In the analysis of ramp event detection systems, Barbour et al[20] defined a "Core Ramp as a 20% change in project power in a 30 minute period or less". This definition was extended to include the period before and after the core ramp event if the intervals experienced a 10% change or greater.

The Bonneville Power Administration has defined a persistent deviation [21] used in determining financial penalties for deviations from scheduled generation. Section 41 (a) will be repeated here.

a) "For Generation Imbalance Service only:

> Negative deviation (actual generation greater than scheduled) or positive deviation (generation is less than scheduled) in the same direction for four or more consecutive hours, if the deviation exceeds both: (i) 15% of the schedule for the hour, and (ii) 20 MW in each hour. All such hours will be considered a Persistent Deviation."

Following the BPA persistent deviation statement the ramp detection mechanism will indicate ramp events of 20MW or greater over a one hour time interval. Note that the focus of this research is not to build a BPA Persistent Deviation detector but rather a wind power ramp detector for an ESS. Upward ramps and downward ramps will be detected and indicated in the output.

## 4.3 Power Ramp Rate

For the purposes of this research the Zhang definition will be used without taking the absolute value of the power difference.

$$PRR = \frac{P(T + \Delta T) - P(T)}{\Delta T} \tag{21}$$

When PRR is negative a downward ramp is found and an upward ramp is a positive PRR. A one-hour time difference will be used and the PRR threshold will be set at 20MW.

# 5 Fuzzy Inference System

The detection of PRRs of 20 MW and greater is accomplished by a Fuzzy Inference System (FSS). A fuzzy logic system offers simplicity of design and implementation and allows a more intuitive approach to solving certain classes of problems than brute force programming.

## 5.1 Overview

The primary components for the FIS are shown in Figure 5.1, which was adapted from Passino and Yurkovich's book on Fuzzy Control [22]. The fuzzification block is a process that converts the input from crisp values (numeric values) into fuzzy sets through the use of membership functions. The inference mechanism works in association with the rule-base to determine the extent of relevance each rule has to the current input. Passino calls this process "matching". [22] Additionally, the inference mechanism "draws conclusions using the current inputs and the information in the rule base." [22]

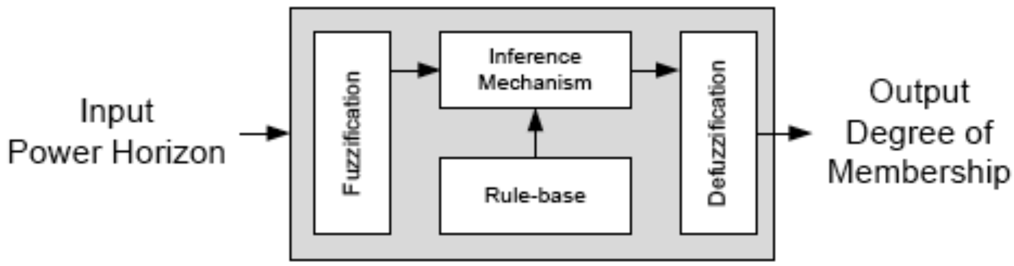


Figure 5.1: Fuzzy Inference Architecture

The defuzzification process converts the output from the inference mechanism to crisp outputs. There are a number of methods that can be used to arrive at a crisp output and are discussed in length in Passino's book [22].

MATLAB uses a Mamdani's fuzzy inference method for its fuzzy toolbox and operates much like the above description with the exception on how it handles the output section [23]. This will be discussed in the section below.

## 5.2 The Power Ramp Detector

The FIS system for this research is a single input single output implementation. The input is the PRR from section 4.3 and it represents the change in power --in P.U.-- with respect to time, dP/dt. The name given to the input is fuzzyDelta. The base for the P.U. is 100MW and the wind farm can generate up to ~120MW. The delta time will be one hour, so if the power changes from 0 to full scale in one hour or less, the PRR will range from 0 to ~1.2 P.U.. The input membership function in Figure 5.2 ranges from -2 to 2. The upper and lower boundaries could have been made tighter, however, there is no harm in a broader boundary. The noRamp section was set to give a dead zone or a zero output when the dP/dt is below the 20MW/hr level.

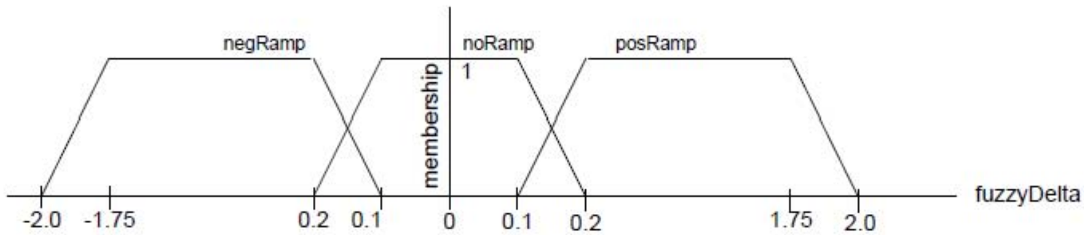


Figure 5.2: Input Membership Functions

The output is named rampDetect and its membership function is rather straightforward as seen in Figure 5.3. The inference system using the rule set generates a fuzzy set that is used to determine the degree of membership according the output membership function. The rampDetect signal has a range from -1 to 1 representing a 20MW/hr or greater downward ramp or a 20MW/hr or greater upward ramp respectively.

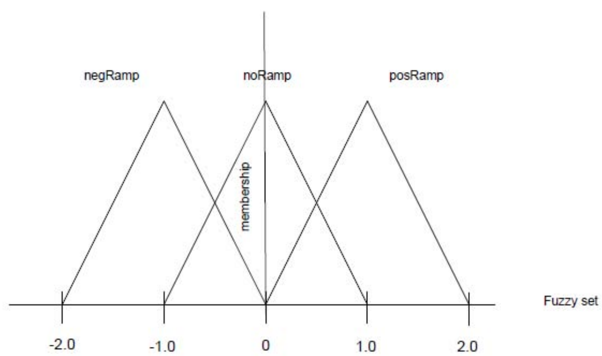


Figure 5.3: Output Membership Function

The rule set guides the inference system in determining how to handle the input, which rules apply, and creates the fuzzy set for the output membership function. The rule set is usually expressed in “modus ponens” or If-Then statements [22] and the rules for the ramp detector are stated below:

1. If (fuzzyDelta is posRamp) then (rampDetect is posRamp)
2. If (fuzzyDelta is noRamp) then (rampDetect is noRamp)
3. If (fuzzyDelta is negRamp) then (rampDetect is negRamp)

## 5.3 Fuzzy Detector Results

The fuzzy detector was run on the output of Model 1A for the 6$^{th}$ horizon (one-hour) Figure 5.4 and the two-hour ahead 12$^{th}$ horizon Figure 5.5. Bold red highlights were outlined for the one-hour case and the two-hour case to indicate where the prediction was made. The fuzzy detector gives a sharp well-defined indication of the downward ramp in both the one-hour and two-hour cases. Predicting the leading edge of the extreme ramp event was not done, but the model did predict the ramp after the wind speed subsided to the turbines operational speed Figure 5.6.

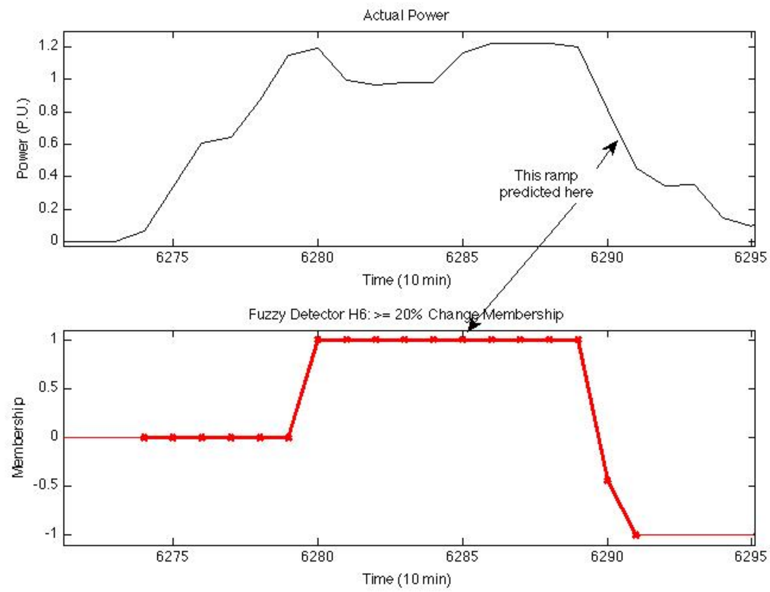


Figure 5.4: Power Ramp Detection, Horizon 6

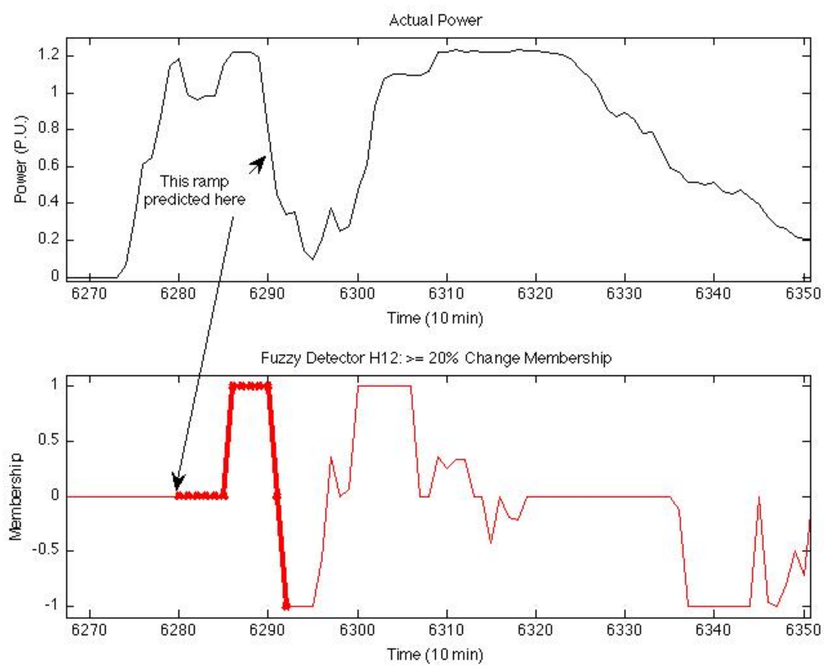


Figure 5.5: Power Ramp Detection, Horizon 12, Extreme Ramp Event

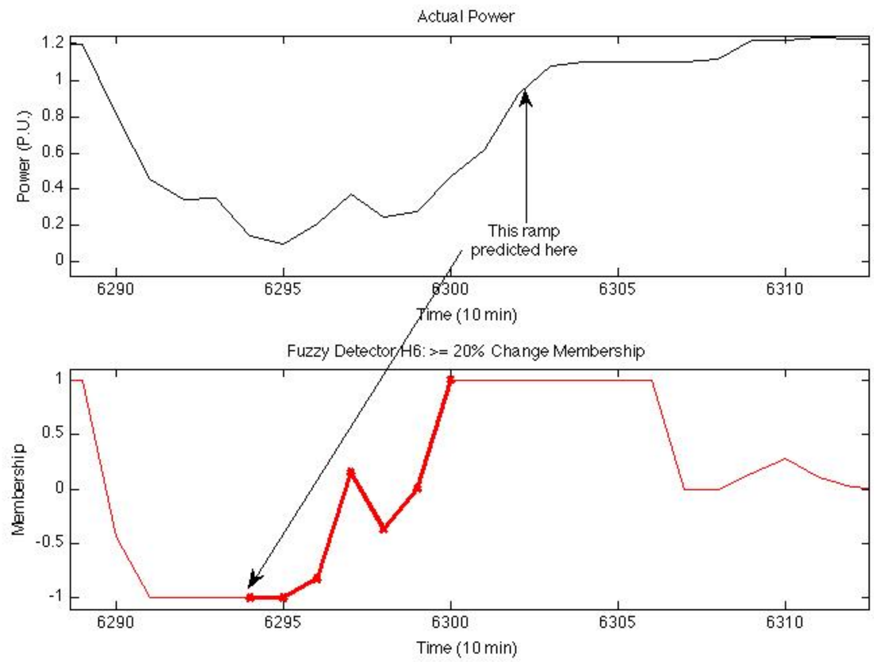


Figure 5.6: Extreme Ramp Recovery Detection, Horizon 6

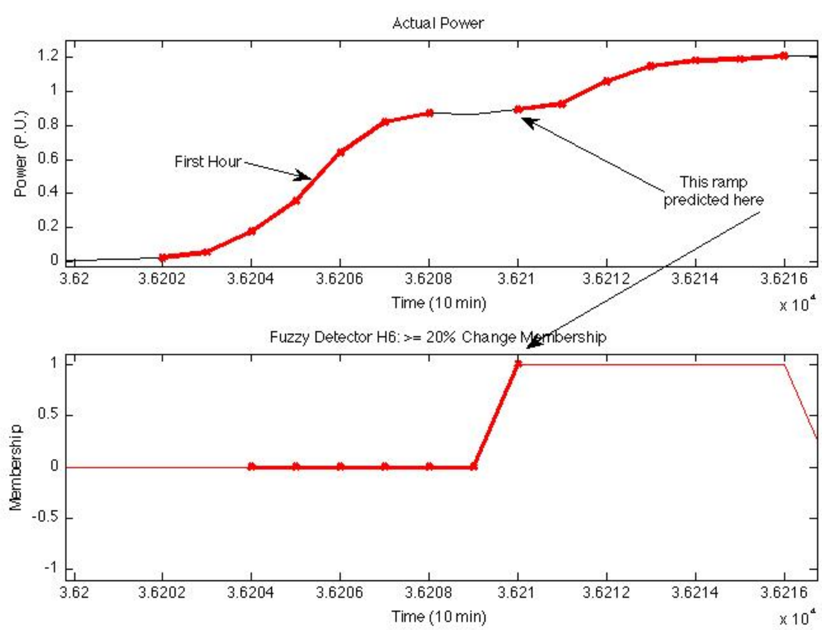


Figure 5.7: Ramp Detection, Horizon 6, Medium Ramp Event

Looking at the medium ramp event Figure 5.7 the ramp detector did not predict the first hour of the ramp. By 30 minutes into the ramp event at time index 36204 the ramp detector was predicting a 20MW or greater ramp to occur at time index 36210. The 12$^{th}$ horizon plot did not add any extra information in the prediction for this ramp event.

The ramp detector could easily be refined to include different degrees of ramp rate as separate outputs.

# 6 Conclusion

Large scale wind energy integration into the Pacific Northwest is a relatively new asset for the area. An energy storage system with a sophisticated control algorithm along with wind power prediction will help manage the production from this renewable resource. This research has investigated several autoregressive moving average models for predicting wind speeds. The predicted results for several horizons and wind ramp events were compared against the persistence model and against other models. Model 1 and Model 3 gave the best predictions and performance would probably increase with the inclusion of wind direction data at the wind farm.

Model 1 was selected to provide wind speed horizons to the wind farm power generation algorithm, which were then processed by a fuzzy logic ramp detector to identify power ramp events.

The detection system worked well for medium and extreme ramp events, but early detection, within the first hour, was not achieved. A measurement method for quantifying the performance of the ramp detector was not developed during this research. Performance was checked by manually selecting ramp events and comparing plots.

## 6.1 Next steps

The investigation of Model 1 and the spinoff models that changed the selection priority of MetStations, with competing favorable wind directions, demonstrated the need for wind direction data at the wind farm. If this data are not directly available from the wind farm owner, then perhaps it could be mined from existing data by looking at the differences in wind velocities from each turbine.

Barometric pressure is another indicator of meteorological events and the information is available in the MetStations data set but not at the wind farm. Perhaps there may be sufficient information in the surrounding MetStations to provide another useful indicator.

Using the mean squared error to measure overall performance gives little information about the performance during ramp events. The fuzzy logic detector could be modified to identify ramp events for wind speed. Once ramp events are identified compute the MSE for only valid ramp events.

The development of metrics to measure the performance of the power ramp detector is needed to provide further insight for design improvements.

# BIBLIOGRAPHY


[1] "WIND_Installed_Capacity_Plot.pdf" http://www.bpa.gov/corporate/WindPower/ .

[2] H. Han, T. K. . Brekken, A. von Jouanne, A. Bistrika, and A. Yokochi, "In-lab research grid for optimization and control of wind and energy storage systems," in *2010 49th IEEE Conference on Decision and Control (CDC)*, 2010, pp. 200-205.

[3] M. Khalid and A. V. Savkin, "Adaptive filtering based short-term wind power prediction with multiple observation points," in *Control and Automation, 2009. ICCA 2009. IEEE International Conference on*, pp. 1547–1552.

[4] M. Khalid and A. V. Savkin, "Adaptive filtering based short-term wind power prediction with multiple observation points," in *Control and Automation, 2009. ICCA 2009. IEEE International Conference on*, pp. 1547–1552.

[5] C. W. Potter and M. Negnevitsky, "Very short-term wind forecasting for Tasmanian power generation," *IEEE Transactions on Power Systems*, vol. 21, no. 2, pp. 965- 972, May 2006.

[6] S. S. Soman, H. Zareipour, O. Malik, and P. Mandal, "A review of wind power and wind speed forecasting methods with different time horizons," in *North American Power Symposium (NAPS), 2010*, 2010, pp. 1-8.

[7] S. Rajagopalan and S. Santoso, "Wind power forecasting and error analysis using the autoregressive moving average modeling," in *IEEE Power & Energy Society General Meeting, 2009. PES '09*, 2009, pp. 1-6.

[8] M. S. Miranda and R. W. Dunn, "One-hour-ahead wind speed prediction using a Bayesian methodology," in *Power Engineering Society General Meeting, 2006. IEEE*, 2006, p. 6–pp.

[9] J. L. Torres, A. García, M. De Blas, and A. De Francisco, "Forecast of hourly average wind speed with ARMA models in Navarre (Spain)," *Solar Energy*, vol. 79, no. 1, pp. 65-77, Jul. 2005.

[10] L. Kamal and Y. Z. Jafri, "Time series models to simulate and forecast hourly averaged wind speed in Quetta, Pakistan," *Solar Energy*, vol. 61, no. 1, pp. 23-32, Jul. 1997.

[11] U. Schlink and G. Tetzlaff, "Wind Speed Forecasting from 1 to 30 Minutes," *Theoretical and Applied Climatology*, vol. 60, no. 1-4, pp. 191-198, Sep. 1998.

[12] P. Poggi, M. Muselli, G. Notton, C. Cristofari, and A. Louche, "Forecasting and simulating wind speed in Corsica by using an autoregressive model," *Energy Conversion and Management*, vol. 44, no. 20, pp. 3177-3196, Dec. 2003.

[13] J. Andrews and N. Jelley, *Energy Science: principles, technologies, and impacts*. New York: Oxford University Press Inc., 2007.

[14] *A Linear Systems Primer*. Boston, MA: Birkhäuser Boston, 2007.

[15] "Inverses and Determinants Linear Algebra (MATLAB®).pdf," *Inverses and Determinants:: Linear Algebra*. [Online]. Available: http://www.mathworks.com/help/techdoc/math/f4-2224.html.

[16] Vestas, “Vestas V821_65_UK Product Brochure.pdf,” *Vestas Search Results*. [Online]. Available: http://www.vestas.com/Default.aspx?ID=9203&q=v821_65_UK.

[17] Z. Z. Yen, “Analysis and optimal sizing of an energy storage system for wind farm applications,” Thesis/Dissertation.

[18] C. Kamath, “Understanding wind ramp events through analysis of historical data,” in *Transmission and Distribution Conference and Exposition, 2010 IEEE PES*, 2010, pp. 1–6.

[19] H. Zheng and A. Kusiak, “Prediction of Wind Farm Power Ramp Rates: A Data-Mining Approach,” *Journal of Solar Energy Engineering*, vol. 131, p. 031011, 2009.

[20] Philip L. Barbour, Sean Casey, and Stel N. Walker, Ph.D., “Evaluation of BPA Vendors Wind Plant ‘Wind Ramp Event’ Tracking System.”Energy Resources Research Laboratory, Department of Mechanical Engineering, Oregon State University, 21-Jun-2010.

[21]“2010 Wholesale Power and Transmission Rate Adjustment Proceeding (BPA-10) Administratior’s Final Record of Decision Appendix C.” Bonneville Power Administration, Jul-2009.

[22] K. Passino and S. Yurkovich, *Fuzzy Control*. Menlo Park, CA: Addison Wesley Longman, Inc, 1998.

[23]“Matlab Fuzzy Inference Systems,” *Fuzzy Inference Systems::Tutorial*. [Online]. Available: http://www.mathworks.com/help/toolbox/fuzzy/fp351dup8.html.